Faulting and Folding of the Transgressive Surface Offshore Ventura Records Deformational Events in the Holocene

Hector Perea[1,2,3]*, Gülsen Ucarkus[4], Neal Driscoll[2], Graham Kent[5], Yuval Levy[2,6] and Thomas Rockwell[6]

[1]Facultad de Ciencias Geológicas, Universidad Complutense de Madrid, Madrid, Spain, [2]Geosciences Research Division, Scripps Institution of Oceanography, University of California, San Diego, San Diego, CA, United States, [3]Institut de Ciències del Mar, Consejo Superior de Investigaciones Científicas, Barcelona, Spain, [4]Geological Engineering Department, Istanbul Technical University, Istanbul, Turkey, [5]Nevada Seismological Laboratory, University of Nevada, Reno, Reno, NV, United States, [6]Department of Geological Sciences, San Diego State University, San Diego, CA, United States

Identifying the offshore thrust faults of the Western Transverse Ranges that could produce large earthquakes and seafloor uplift is essential to assess potential geohazards for the region. The Western Transverse Ranges in southern California are an E-W trending fold-and-thrust system that extends offshore west of Ventura. Using a high-resolution seismic CHIRP dataset, we have identified the Last Glacial Transgressive Surface (LGTS) and two Holocene seismostratigraphic units. Deformation of the LGTS, together with onlapping packages that exhibit divergence and rotation across the active structures, provide evidence for three to four deformational events with vertical uplifts ranging from 1 to 10 m. Based on the depth of the LGTS and the Holocene sediment thickness, age estimates for the deformational events reveal a good correlation with the onshore paleoseismological results for the Ventura-Pitas Point fault and the Ventura-Avenue anticline. The observed deformation along the offshore segments of the Ventura-Pitas Point fault and Ventura-Avenue anticline trend diminishes toward the west. Farther north, the deformation along the offshore Red Mountain anticline also diminishes to the west with the shortening stepping north onto the Mesa-Rincon Creek fault system. These observations suggest that offshore deformation along the fault-fold structures moving westward is systematically stepping to the north toward the hinterland. The decrease in the amount of deformation along the frontal structures towards the west corresponds to an increase in deformation along the hinterland fold systems, which could result from a connection of the fault strands at depth. A connection at depth of the northward dipping thrusts to a regional master detachment may explain the apparent jump of the deformation moving west, from the Ventura-Pitas Point fault and the Ventura-Avenue anticline to the Red Mountain anticline, and then, from the Red Mountain anticline to the Mesa-Rincon Creek fold system. Finally, considering the maximum vertical uplift estimated for events on these structures (max ~10 m), along with the potential of a common master detachment that may rupture in concert, this system could generate a large magnitude earthquake (>Mw 7.0) and a consequent tsunami.

INTRODUCTION

The Sumatra 2004 and Tohoku 2011 earthquakes and consequent tsunamis (Ammon et al., 2005; Bilham, 2005; Lay et al., 2005; Subarya et al., 2006; Ide et al., 2011; Ozawa et al., 2011; Sato et al., 2011; Simons et al., 2011) brought into sharp focus the need to understand better geohazards along convergent margins. In addition, multifault earthquake ruptures, as observed in the 2016 Kaikoura Earthquake in New Zealand (Clark et al., 2017; Hamling et al., 2017; Kaiser et al., 2017; Stirling et al., 2017; Litchfield et al., 2018), reveal complex and cascading fault linkages that control rupture lengths and potential earthquake magnitudes. Advances in high-resolution geophysical imaging (i.e., seismic reflection and swath-bathymetry) provide unprecedented resolution of the offshore deformation and fault architecture; such technological developments allow for improved imaging of fault offsets and their recency (Armijo et al., 2005; McNeill et al., 2007; Barnes, 2009; Brothers et al., 2009, 2011; Barnes and Pondard, 2010; Perea et al., 2012; Polonia et al., 2012; McNeill and Henstock, 2014; Escartín et al., 2016; Sahakian et al., 2017; Perea et al., 2018; Gràcia et al., 2019).

In Southern California, the central and Western Transverse Ranges are characterized by a series of east-west trending south verging fold-and-thrust fault systems that bound the Santa Barbara Channel and Ventura Basin to the north (Jackson, 1981; Yeats, 1983; Yeats and Olson, 1984; Grigsby, 1986; Yeats et al., 1987, 1988; Yerkes et al., 1987; Yerkes and Lee, 1987; Namson and Davis, 1988; Rockwell, 1988; Hubbard et al., 2014; Levy et al., 2019). Paleoseismological studies have characterized the Holocene earthquake history in the region, concluding that there is the potential to generate large magnitude earthquakes (M > 7.0) (Rockwell et al., 1988, 2016; Dolan and Rockwell, 2001; McAuliffe et al., 2015). The offshore extent and character of the thrust fault-fold systems associated with the Western Transverse Ranges (e.g., Ventura-Avenue anticline or Ventura-Pitas Point fault) remain uncertain in the near-shore region (Dahlen et al., 1990; Sorlien et al., 2000, 2014; Plesch et al., 2007; Hubbard et al., 2014; Sorlien and Nicholson, 2015; Nicholson et al., 2016; Rockwell et al., 2016; Johnson et al., 2017b).

In this study, we present new high-resolution CHIRP seismic data together with reprocessed sparker data to define the occurrence of Holocene deformation in the offshore Western Transverse Ranges between Ventura and Santa Barbara (**Figure 1**). Interpretation of these new shallow geophysical data places important constraints on the seafloor deformation during the last ~10–12 ka related to several geological structures in the Offshore Ventura and Inner Santa Barbara basins. In addition, it allows us to correlate the identified offshore uplift events with the well-documented onshore Holocene paleoearthquakes. Examination of the nested geophysical offshore surveys may also provide insight into the structural relationship between the Holocene deformation observed in the surficial stratal geometry and seafloor morphology and the deeper

structures associated with this deformation. Such structural and stratigraphic studies in convergent settings have both societal and scientific relevance as they allow us to examine how thrust fault and fold propagation controls continental margin architecture as well as to assess the potential seismic and tsunamigenic hazard associated with thrust fault systems.

GEOLOGICAL SETTING: OFFSHORE VENTURA AND SANTA BARBARA BASINS

The Transverse Ranges have experienced different phases of tectonic deformation related to the evolution of the western Pacific-North America plate boundary for the past 25 Ma (e.g., Yerkes and Lee, 1987; Sedlock and Hamilton, 1991; Nicholson et al., 1994). During the past 3–5 Ma the area has been subjected to N-S compression related to the incremental formation of a regional restraining bend in the San Andreas Fault system and resulting in the development of an E-W trending fold-and-thrust belt system (e.g., Dibblee, 1982; Yerkes and Lee, 1987; Levy et al., 2019).

Within the Western Transverse Ranges are the eastward trending Ventura sedimentary basin and its offshore extension (**Figure 1**), which is infilled by more than 5 km of Pleistocene sediment (e.g., Fischer, 1976; Yeats, 1983; Yerkes et al., 1987; Yeats et al., 1988; Huftile and Yeats, 1995; Rockwell et al., 2016). A series of folds and thrusts bounds the basin. To the south, the main structure is the Oak Ridge anticline, which is associated with a reverse fault that dips steeply to the south and continues westward offshore, and has a slip rate ranging from 2.6 to 5 mm/yr during the Quaternary that diminishes towards the west (e.g., Yerkes et al., 1987; Yeats et al., 1988; Shaw and Suppe, 1994; Huftile and Yeats, 1995; Sorlien et al., 2000; Azor et al., 2002; Plesch et al., 2007). To the north, there is a series of E-W anticlines verging south, associated with reverse faults dipping to the north. The main structures are the Ventura-Pitas Point fault, the Ventura-Avenue anticline trend (also identified as the Rincon or Dos Cuadras anticline in the offshore), the Red Mountain fault and the San Cayetano fault, which have average slip-rates between 2 and 6 mm/yr for the Quaternary (Yeats et al., 1987; Yerkes et al., 1987; Rockwell, 1988; Rockwell et al., 1988; Huftile and Yeats, 1995; Plesch et al., 2007; Hubbard et al., 2014).

Geodetic data reveal north-south convergence across the Ventura Basin at ~7–10 mm/yr (Donnellan et al., 1993a, 1993b; Hager et al., 1999; Marshall et al., 2013). In addition, the inversion of horizontal GPS velocities in the whole Western Transverse Ranges show fast contraction rates along the southernmost Ventura Basin, decreasing both to the west and east (Marshall et al., 2013). In spite of the availability of continuous GPS data in the Channel Islands, the inversion method cannot resolve the specific offshore structures where the shortening is being accommodated, which limits the confidence of the GPS velocities derived from the horizontal
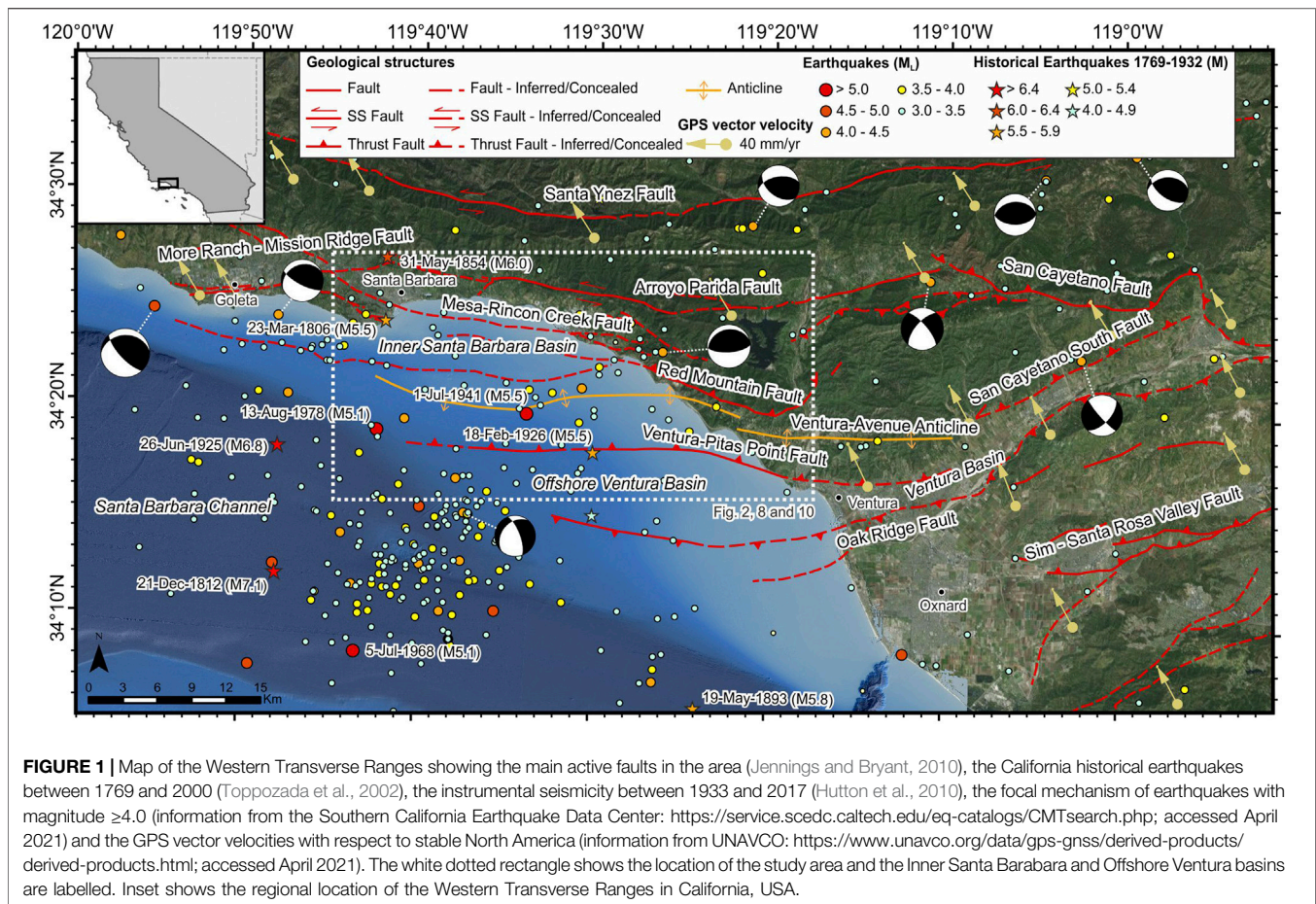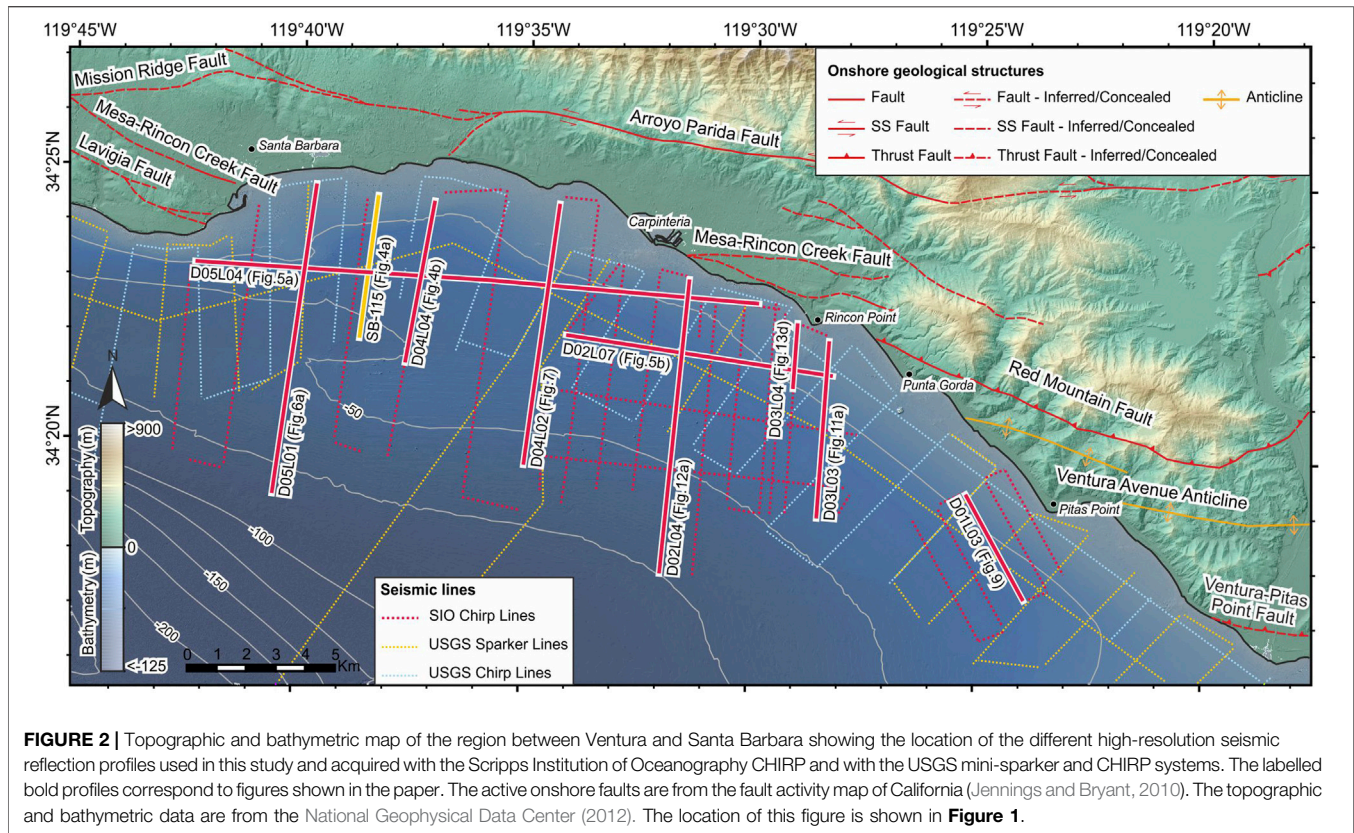
FIGURE 1 | Map of the Western Transverse Ranges showing the main active faults in the area (Jennings and Bryant, 2010), the California historical earthquakes between 1769 and 2000 (Toppozada et al., 2002), the instrumental seismicity between 1933 and 2017 (Hutton et al., 2010), the focal mechanism of earthquakes with magnitude ≥4.0 (information from the Southern California Earthquake Data Center: https://service.scedc.caltech.edu/eq-catalogs/CMTsearch.php; accessed April 2021) and the GPS vector velocities with respect to stable North America (information from UNAVCO: https://www.unavco.org/data/gps-gnss/derived-products/derived-products.html; accessed April 2021). The white dotted rectangle shows the location of the study area and the Inner Santa Barabara and Offshore Ventura basins are labelled. Inset shows the regional location of the Western Transverse Ranges in California, USA.

inversion. Consequently, zones with localized fast contraction offshore of the Ventura Basin trend cannot be discarded as predicted by interseismic strain modelling (Marshall et al., 2013).

The seismicity along the Ventura Basin and the Santa Barbara Channel is moderate, both in terms of earthquake frequency and magnitude and mainly shallow, between 3 and 15 km (Hutton et al., 1991). Large earthquakes with magnitudes above 6.0 have occurred in the area since the XVIII century as the December 21, 1812 (M7.1), the May 31, 1854 (M6.0) and the June 26, 1925 (M6.8) (Toppozada et al., 2002; Hutton et al., 2010) (**Figure 1**); however it has been discussed that the 1812 event may have been related to a rupture along the San Andreas fault and probably triggered by the December 8, 1812 earthquake that ruptured approximately between Pallett Creek and Cajon Pass (Toppozada et al., 2002; Toppozada and Branum, 2004). The distribution of the instrumental seismicity (colored circles in **Figure 1**) shows an area with a high density of earthquakes within the Santa Barbara Channel, south of Santa Barbara, although most of them occurred in 1941 and 1968 and, thus, probably corresponding to the aftershock sequence of the July 1, 1941 (M 5.5) and the July 5, 1968 (M5.1) events (**Figure 1**). Most of the earthquakes focal mechanisms in the area show a predominance of reverse faulting on west to northwest striking nodal planes, which is consistent with the observations from the geodetic data (**Figure 1**).

Paleoseismological studies performed on structures along the northern boundary of the Ventura basin show evidence for surface vertical slip during the Upper Pleistocene and Holocene. Dolan and Rockwell (2001) identified the last earthquake occurred in the eastern part of the San Cayetano fault, which produced 4.3 m of surface slip. The event occurred after 1660 CE and these autohrs proposed that could correspond to the December 21, 1812 event; however, as mentioned before, the 1812 earthquake could have been produced by the San Andreas fault (Toppozada et al., 2002; Toppozada and Branum, 2004). A study carried out in the Punta Gorda marine terrace revealed that the terrace was vertically separated 34 m across the Red Mountain fault system and that the slip may have occurred in the last 45 ka (Lindvall et al., 2002). Also analyzing marine terraces between Punta Gorda and Pitas Point, Rockwell et al. (2016) found evidence of four vertical uplift events related to the Ventura Avenue anticline. The events occurred between 0.95 and 6.7 kys BP and produced vertical uplifts between 5 and 12 m. To the south of Pitas Pont, McAuliffe et al. (2015) carried on a paleoseismological study acquiring and interpreting geotechnical and geophysical data across the Ventura-Pitas Point fault in the city of Ventura. They found evidence that at least two deformation events occurred in the last 4.7 ka and produced vertical uplift between 4.5 and 6.5 m.

FIGURE 2 | Topographic and bathymetric map of the region between Ventura and Santa Barbara showing the location of the different high-resolution seismic reflection profiles used in this study and acquired with the Scripps Institution of Oceanography CHIRP and with the USGS mini-sparker and CHIRP systems. The labelled bold profiles correspond to figures shown in the paper. The active onshore faults are from the fault activity map of California (Jennings and Bryant, 2010). The topographic and bathymetric data are from the National Geophysical Data Center (2012). The location of this figure is shown in **Figure 1**.

DATA AND METHODS

Seismic Data

Newly acquired Compressed High Intensity Radar Pulse (CHIRP) profiles and USGS mini-sparker and CHIRP profiles (Sliter et al., 2008; Johnson et al., 2017a) have been interpreted in this study (**Figure 2**). The CHIRP data were acquired onboard the Scripps Institution of Oceanography R/V Point Loma in 2013 using a 1–15 kHz pulse swept over 50 ms. These profiles have decimeter vertical resolution, 40–60 m of sub-bottom penetration and cover two different areas in the Santa Barbara Channel. In the area between Rincon Point and Santa Barbara, sixteen dip profiles were acquired beginning or ending close to the coastline and approximately perpendicular to it, with lengths between 5 and 10 km, and four strike lines parallel to the coastline and crossing the dip lines to correlate the acoustic units throughout the study area (**Figure 3**). A series of five profiles, trending NW-SE, with an average length of 4.5 km, were acquired close to Pitas Point (**Supplementary Figure S3**). All the newly acquired CHIRP profiles were processed using the SIOSEIS software. The designed processing flow consisted of four different steps that first reordered the seg-y headers, filtered the shots, determined signal amplitude values, picked seafloor with tracking, corrected time shift due to swell, improved amplitude with a gain function and mixing with previous shots, and muted the water column signal and produced the final seg-y file.

The USGS profiles were acquired in the region between Goleta and Oxnard (**Figures 1**, **2**). They were collected as part of the California Seafloor Mapping Program between 2007 and 2008
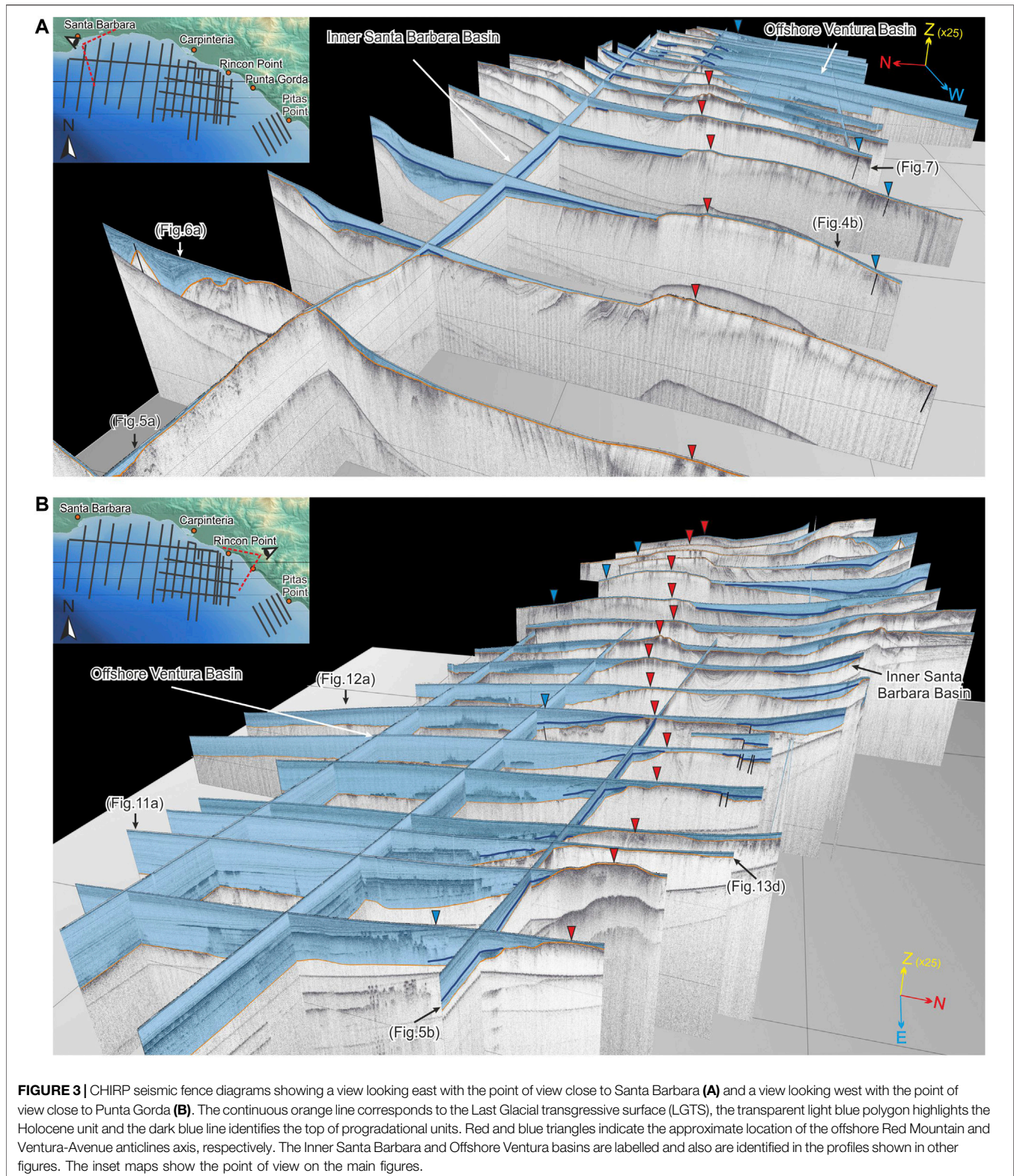
aboard the R/V Zephyr and R/V Parke Snavely (Sliter et al., 2008; Johnson et al., 2017a). These profiles were acquired perpendicular to the coastline, spaced 1.0–1.5 km apart and used a SIG 2Mille mini-sparker and an Edgetech SB-0512i CHIRP systems. The sparker profiles have a sub-bottom penetration of ~200 m with a 2–3 m vertical resolution, whereas the chirp profiles penetrate up to 60 m below the seafloor and have decimeter vertical resolution.

All the high-resolution seismic profiles were uploaded into Kingdom and Fledermaus software packages for interpretation, and to correlate structures and horizons throughout the data volume.

Approaches to Calculate the Holocene Sedimentation Rates and Event Horizon Ages

To determine the probable age of vertical uplift horizon events identified in CHIRP profiles, we estimated the sedimentation rate at different locations along profiles. Knowing the depth of the event horizon and the sedimentation rate it is possible to estimate the age of the horizon. The approach used to calculate the sedimentation rate considers the age of a regional unconformity surface at a certain depth, which has been associated to the Last Glacial Transgression surface (*see* **section 4.1**), at specific locations with the sediment thickness above this surface corresponding to the Holocene deposit.

The age of the regional unconformity surface was estimated measuring its depth below the present sea level at determined location and crossing this depth with different sea level curves for the Holocene (Fairbanks, 1989; Stanford et al., 2011; Muhs et al., 2014; Reeder-Myers et al., 2015; Reynolds and Simms, 2015; Johnson

FIGURE 3 | CHIRP seismic fence diagrams showing a view looking east with the point of view close to Santa Barbara **(A)** and a view looking west with the point of view close to Punta Gorda **(B)**. The continuous orange line corresponds to the Last Glacial transgressive surface (LGTS), the transparent light blue polygon highlights the Holocene unit and the dark blue line identifies the top of progradational units. Red and blue triangles indicate the approximate location of the offshore Red Mountain and Ventura-Avenue anticlines axis, respectively. The Inner Santa Barbara and Offshore Ventura basins are labelled and also are identified in the profiles shown in other figures. The inset maps show the point of view on the main figures.

et al., 2017b). This provided a maximum and minimum age for the regional unconformity surface at each location, thus incorporating the uncertainty of the approach in the analysis. The thickness of the Holocene deposit was obtained measuring the distance between the

seafloor and the regional unconformity surface at the same locations where the age of this surface was estimated. To transform the width from time to depth we used a nominal interval velocity of 1500 m/s TWTT. All calculations were performed approximately 1000 m

south of the deformation zones, to avoid thickness variations related to fault activity. In addition, the calculations were determined at two different offsets along the CHIRP profiles distanced 500 m one from the other to average the results. Knowing the Holocene sediment thickness and the range of possible ages of the regional unconformity surface, we obtained minimum and maximum sedimentation rates (**Supplementary Table S1**).

To calculate the age of the different interpreted event horizons it is necessary to estimate the thickness of the sedimentary units between the seafloor and the event horizon and the sedimentation rate at each site of interest. Likewise, we have used a nominal interval velocity of 1500 m/s TWTT to determine the thickness in meters. Considering the maximum and minimum Holocene sedimentation rates, we have obtained the maximum and minimum age for each event horizon (**Supplementary Tables S2, S3**).

Approaches to Estimate the Vertical Uplift for the Identified Deformation Events

Two different approaches were used to estimate the vertical uplift for the identified event horizons. The first approach measured the cumulative height of fold scarp. To accomplish this, we assumed that the regional seafloor slope of the event horizons corresponds to the depositional slope on the downthrown block, considering that this would be the zone with less deformation, which would have a similar slope on top of the uplifted or folded area. Accordingly, the vertical distance between the slope lines on the upthrown and downthrown blocks may record the cumulative vertical uplift (**Supplementary Figure S1**). In the case of the most recent event, the cumulative scarp height (**Supplementary Figure S1B**) would record the vertical uplift of the most recent event. For older events, the cumulative scarp height would equal the older event (event 2) plus the more recent event (event 1; **Supplementary Figure S1C** In order to determine the uplift related to older events, the deformation associated with younger events needs to be subtracted (**Supplementary Figure S1**).

The second approach used to estimate the vertical uplift consisted of measuring the cumulative height of anticline and syncline hinges on a fold system. The approach assumes that the event horizon, which is at present folded, would had been flat, even it may be slightly dipping to the south, before the occurrence of the event. Then, the difference in height between the anticline and the syncline hinges would be the result of the cumulative uplift of this event, or the cumulative uplift if more recent events would have occurred, and assuming no erosion (**Supplementary Figure S2**). Similarly as in the previous approach, when the measured uplift corresponds to more than one event, the specific event vertical uplift is obtain by subtraction of the uplifts determined for the more recent events.

RESULTS

Seismic Stratigraphy

In the seismic profiles, we have identified two different seismostratigraphic units separated by a regional surface with observed truncation (**Figures 3–7**).
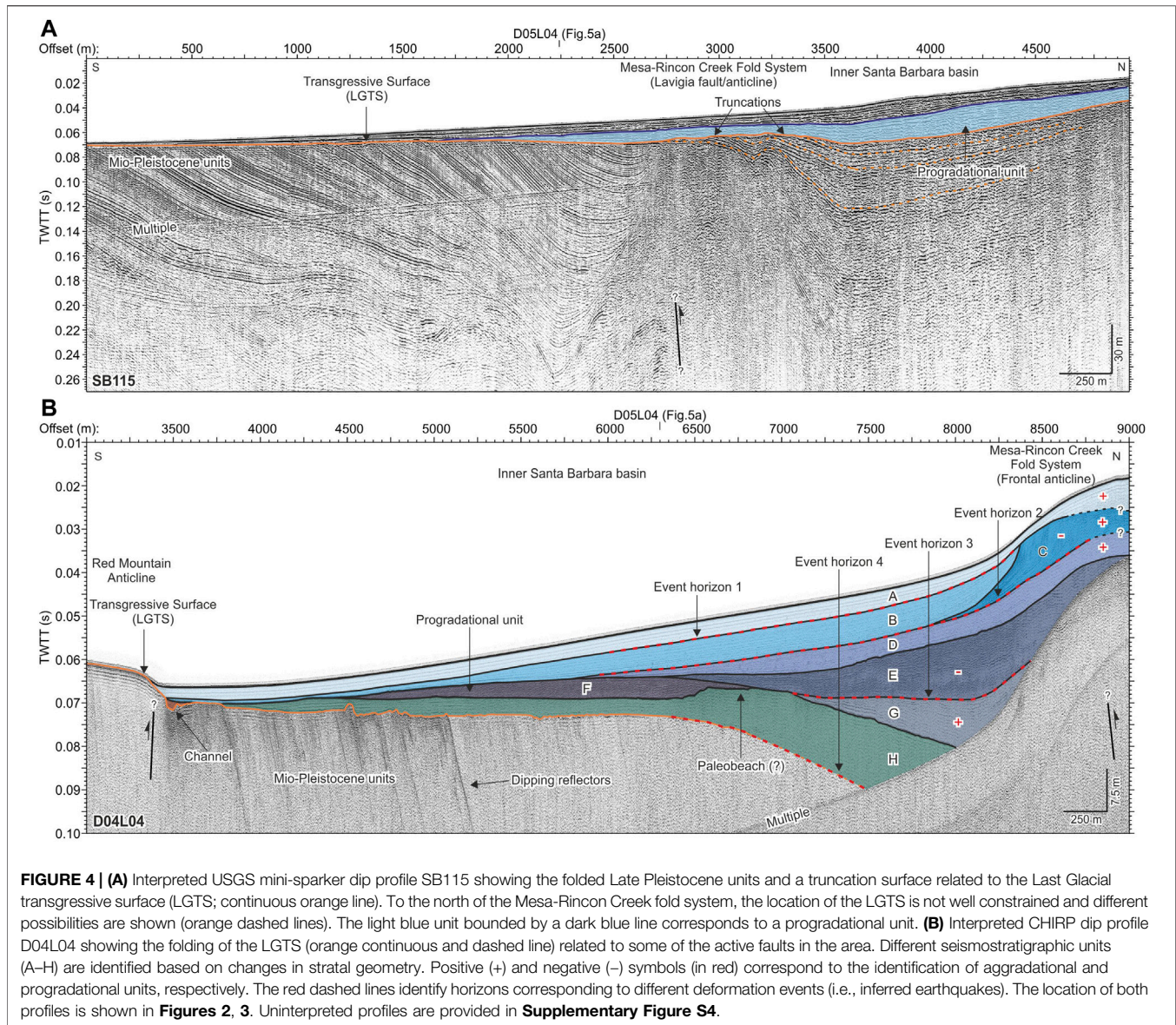
Regional Erosional Unconformity: The Last Glacial Transgressive Surface

A regional unconformity, characterized by a high amplitude reflector with low frequency, is rather continuous and planar throughout the study region (**Figure 3**). The erosive nature of this unconformity is shown by a marked angular unconformity between the reflectors below and above (**Figures 4A**, **5**, **7**) and by the identification of buried ridges (offsets 250–950 in **Figure 5B**). The unconformity at its seaward extent is above 0.1 s two-way travel time (TWTT), a depth equivalent to ~75 m below present sea level (bpsl) using a nominal interval velocity of 1500 m/s TWTT, and the unconformity systematically shallows towards the coast in the acquired profiles. Given that the regional global sea level during the Last Glacial Maximum (LGM; 20–22 ka) was 111–124 m bpsl (Fairbanks, 1989; Stanford et al., 2011; Muhs et al., 2014; Reeder-Myers et al., 2015; Reynolds and Simms, 2015; Johnson et al., 2017b) and that the shelf between Santa Barbara and Ventura was subaerially exposed during the LGM (Johnson et al., 2017b), this unconformity appears to be formed after the LGM during the subsequent sea level rise. The unconformity has been identified in almost all the seismic profiles, with the exception of those located close to the Ventura coastline where the Holocene unit is thicker and the seafloor multiple obscures the deeper reflectors (**Supplementary Figure S3**). Hereafter we refer to this unconformity as the Last Glacial Transgressive Surface (LGTS).

The LGTS exhibits a gentle regional dip towards the south; however, the new CHIRP dataset shows that it has been locally uplifted and folded (**Figures 3**, **4**, **6**, **7**). The structural contour map of the LGTS surface (**Figure 8**) reveals an approximately ENE-WSW to E-W trending elongated ridge that begins at Rincon Point and continues westward across most of the region. Note, its expression in the bathymetry diminishes to the west of Santa Barbara. The uplift of this ridge has created a local E-W trending basin between Santa Barbara and Carpinteria, here we refer to this region as the Inner Santa Barbara Basin (**Figures 1**, **3**). Approximately in the center of this basin, there is a pronounced structural low that coincides with marked deformation of the LGTS (**Figures 3**, **5B**, **8**). Likewise, we refer to the basin to the southeast as the Offshore Ventura Basin (**Figures 1**, **3**); these are subbasins within the larger Santa Barbara Channel.

Pre-LGTS Units (Mio-Pleistocene Units)

Below the LGTS there are the Mio-Pleistocene sedimentary units that show well-developed folds (anticlines and synclines) and high-angle dipping reflectors, where the sedimentary units are imaged (**Figures 4–7**). In some places, these dipping reflectors coincide with irregularities or ridges on the LGTS (offsets 250–950 in **Figure 5B**) that in all likelihood may correspond to hard sedimentary horizons that are more competent. These ridges are also observed along the seafloor bathymetric data in places where the LGTS has been uplifted and exposed. The width of the folds (synclines and anticlines) beneath the LGTS increases

FIGURE 4 | (A) Interpreted USGS mini-sparker dip profile SB115 showing the folded Late Pleistocene units and a truncation surface related to the Last Glacial transgressive surface (LGTS; continuous orange line). To the north of the Mesa-Rincon Creek fold system, the location of the LGTS is not well constrained and different possibilities are shown (orange dashed lines). The light blue unit bounded by a dark blue line corresponds to a progradational unit. **(B)** Interpreted CHIRP dip profile D04L04 showing the folding of the LGTS (orange continuous and dashed line) related to some of the active faults in the area. Different seismostratigraphic units (A–H) are identified based on changes in stratal geometry. Positive (+) and negative (−) symbols (in red) correspond to the identification of aggradational and progradational units, respectively. The red dashed lines identify horizons corresponding to different deformation events (i.e., inferred earthquakes). The location of both profiles is shown in **Figures 2**, **3**. Uninterpreted profiles are provided in **Supplementary Figure S4**.

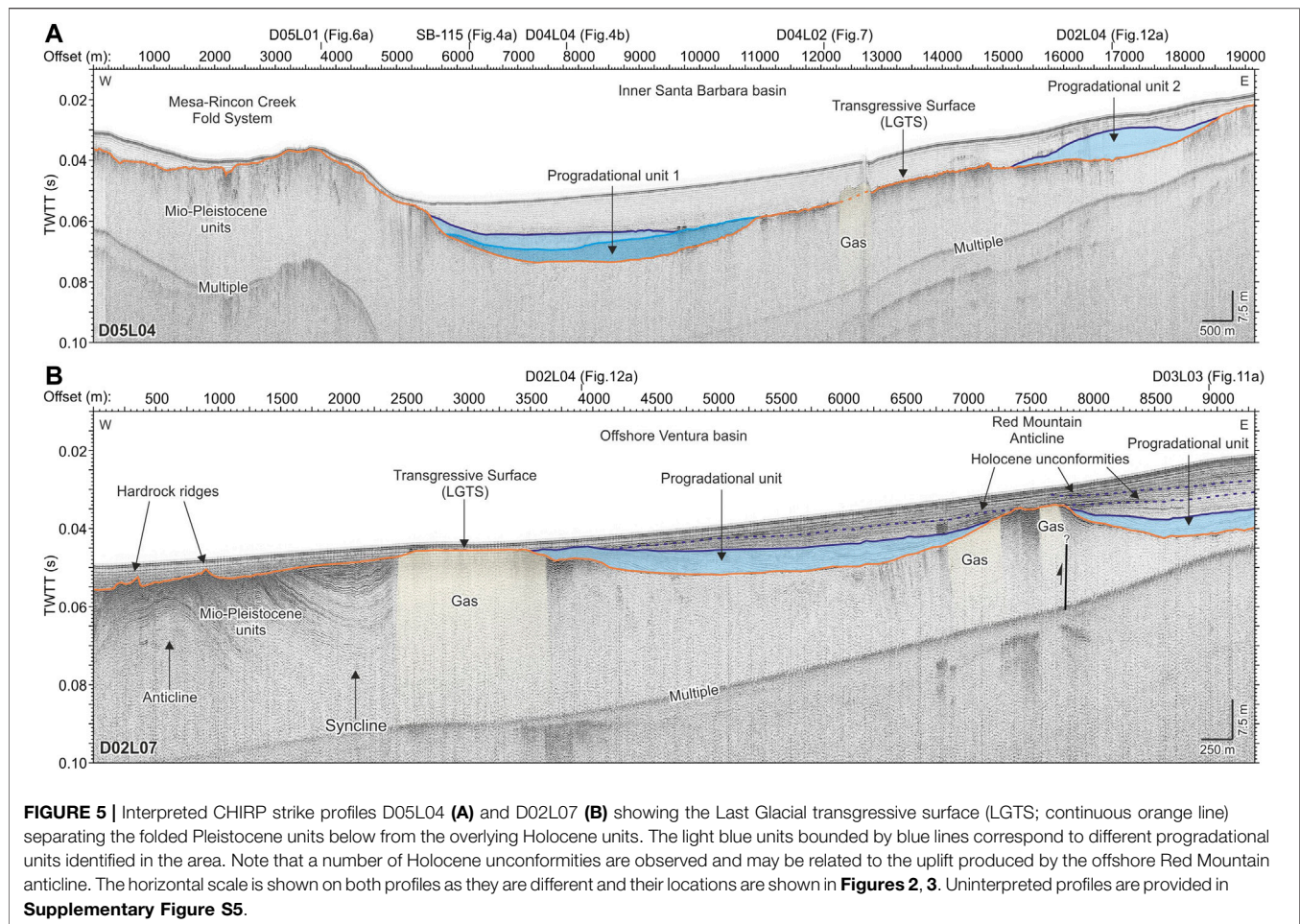and the structural relief across them decrease towards the west (**Figures 3**, **8**).

Holocene Unit

Above the LGTS, there is the Holocene unit, which exhibits marked variation in both distribution and thickness along and across the margin (**Figure 3**). Holocene sediments deposited within the Offshore Ventura and Inner Santa Barbara basins (**Figure 1**), are mostly absent over the E-W anticline separating them. This unit reaches its maximum thickness close to Ventura where the LGTS is not imaged above the multiple (**Figures 9** and **Supplementary Figure S1**). In the strike CHIRP lines shown in **Figure 5**, two different seismic-stratigraphic units are identified. The basal unit is a discontinuous progradational unit characterized by high amplitude and low frequency foreset reflectors and in some locations different progradational units have been identified (**Figures 3**, **4A**, **5**). Usually

these reflectors downlap onto the LGTS, but in some places, they mantle this surface, thus lying disconformable above it. On top of the progradational unit or directly on top of the LGTS, there is an aggradational unit, with continuous and parallel reflectors that exhibit medium to high acoustic amplitude and a high frequency character (**Figures 3**, **4A**, **5**). In localized depocenters of the Inner Santa Barbara Basin (**Figures 4B**, **6**), there exists an expanded stratigraphic section where up to eight seismic-stratigraphic units can be identified. Given the interplay between sedimentation rates and accommodation, the units exhibit either progradation (sedimentation rates > accommodation rates) or aggradation (sedimentation rates < accommodation rates).

Active Structures and Uplift Events

The analyzed seismic dataset exhibits evidence that the LGTS and the Holocene unit have been uplifted and folded (**Figures 3–9**).
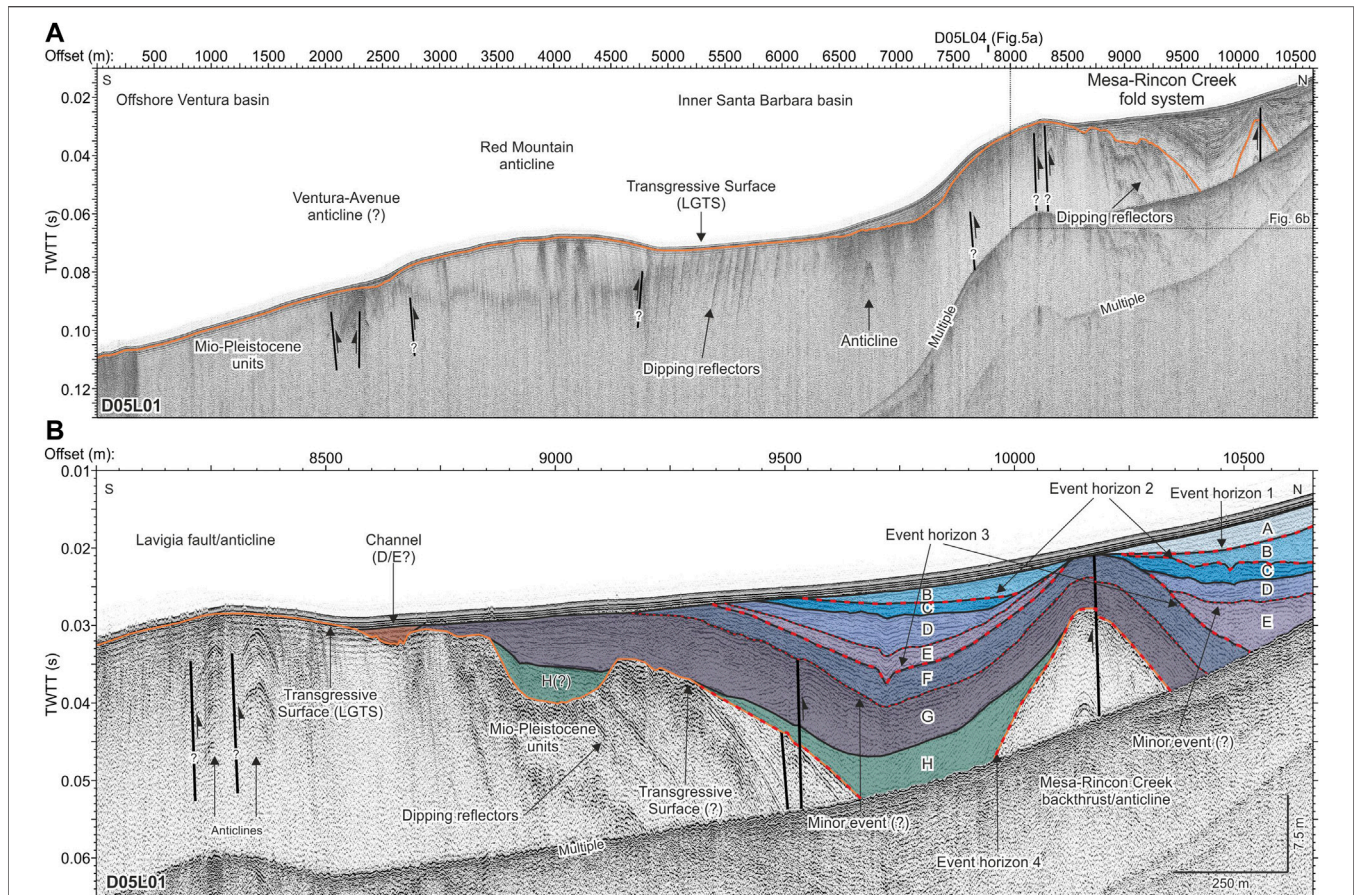
FIGURE 5 | Interpreted CHIRP strike profiles D05L04 **(A)** and D02L07 **(B)** showing the Last Glacial transgressive surface (LGTS; continuous orange line) separating the folded Pleistocene units below from the overlying Holocene units. The light blue units bounded by blue lines correspond to different progradational units identified in the area. Note that a number of Holocene unconformities are observed and may be related to the uplift produced by the offshore Red Mountain anticline. The horizontal scale is shown on both profiles as they are different and their locations are shown in **Figures 2, 3**. Uninterpreted profiles are provided in **Supplementary Figure S5**.

Based on the dense grid of seismic profiles, we have mapped the extent of Late Quaternary active structures, mainly anticlines and synclines across the region (**Figure 10**). Furthermore, the presence of fold scarps, growth strata sequences, onlap unconformities and erosion surfaces in the Holocene unit has allowed for the identification of three to four discrete deformational events.

Ventura-Pitas Point Fault

Offshore of western Ventura, the seismic profiles image a 100 m wide monocline verging to the south that folds the Holocene sediments close to the seafloor, but not the seafloor itself (**Figures 9** and **Supplementary Figure S3**). Towards the west, the height of the monocline diminishes and only deeper Holocene reflectors are folded (**Supplementary Figure S3**). We have mapped this structure for approximately 19 km, from the coastline west to the longitude of Carpinteria (**Figure 10**). Nevertheless, it is important to note that there is uncertainty in the identification of the Ventura-Pitas Point anticline trend between Carpinteria and Punta Gorda given the distance between seismic profiles, the decrease in the structural height of the monocline, and gas wipe-out that obscures acoustic reflectors. Spatially coincident where there is greater uncertainty in identifying the fault and fold, there is a change in trend of the Ventura-Pitas Point fault, from being NW-SE near the coast to E-W farther offshore.

Examination of the CHIRP profiles crossing the Ventura-Pitas Point fault reveals three seismostratigraphic units characterized by growth sequences on the downthrown block and thinning by onlap on the upthrown block that have been progressively folded (i.e., folding attenuates towards the seafloor; **Figure 9**). In addition, the boundary between the different units correspond to an unconformity. In order to calculate the vertical uplift for each event, we assumed that the regional slope of the event horizons corresponds to the depositional slope on the downthrown block and infer it to have similar slope on top of the monocline, and then measure the vertical uplift (first approach explained in **section 3.3**). In addition, to convert two-way travel time (TWTT) to depth, a nominal interval velocity of 1500 m/s TWTT was used because of the lack of available surficial seismic velocities in the area. Accordingly, vertical uplift ranging between 2.8 and 3.0 m, 3.0 and 3.2 m, and 1.5 and 1.6 m were determined for events 1, 2 and 3, respectively (more information in **Supplementary Table S4**). Given that the CHIRP profiles crossing the monocline did not image the LGTS (**Figure 9**), we have not been able to estimate the vertical uplift rates. On the downthrown block and away from the deformation zone, the thickness of unit B between event horizons 1 and 2, and unit C between event horizons 2 and 3 are similar (0.006 s TWTT, approximately 4.7 m, at offset 750 m in **Figure 9**

FIGURE 6 | (A) Interpreted CHIRP strike profile D05L01 showing the folding of the Last Glacial transgressive surface (LGTS; continuous orange line) related to the Mesa-Rincon Creek fold system and offshore Red Mountain anticline. Note that the anticline that is interpreted as the potential Ventura-Avenue anticline is folding the Mio-Pleistocene units, but not the LGTS. The location of the profile is shown in **Figures 2**, **3**. (B) Enlarged section is shown by rectangle in **Figure 6A** highlighting the intense folding of the LGTS (orange continuous line) related to the Mesa-Rincon Creek fold system. Different seismostratigraphic units (A–H) are identified based on stratal geometry. The red dashed lines identify horizons corresponding to different deformation events (i.e., inferred earthquakes). Uninterpreted profiles are provided in **Supplementary Figure S6**.
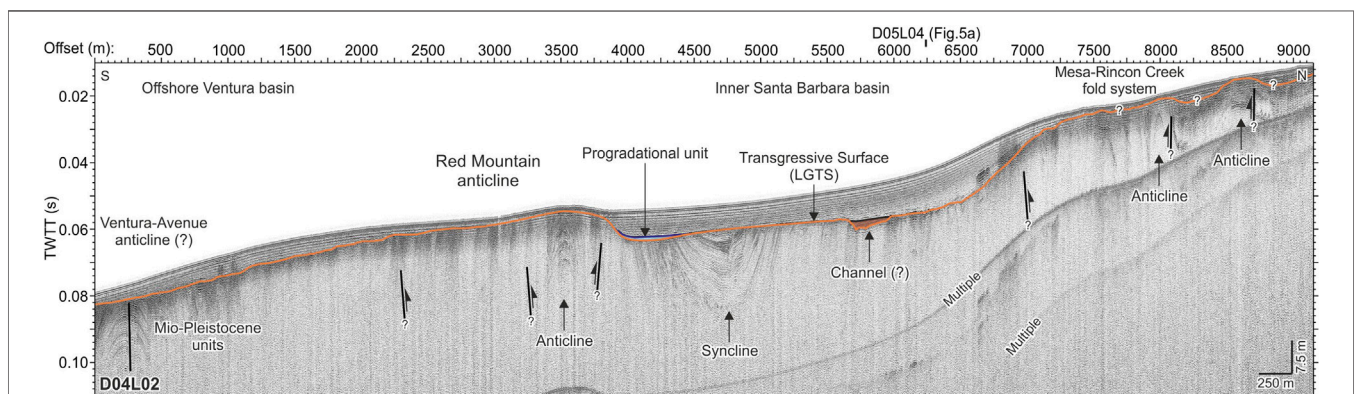
FIGURE 7 | Interpreted CHIRP strike profile D04L02 showing the folding of the Last Glacial transgressive surface (LGTS; continuous orange line) related to the Mesa-Rincon Creek fold system and offshore Red Mountain anticline. The light blue unit bounded by a dark blue line corresponds to a progradational unit and the brown identifies a possible channel. Note that the identified Ventura-Avenue anticline is clearly folding the Pleistocene units but not the LGTS. The location of the profile is shown in **Figures 2**, **3**. Uninterpreted profile is provided in **Supplementary Figure S7**.
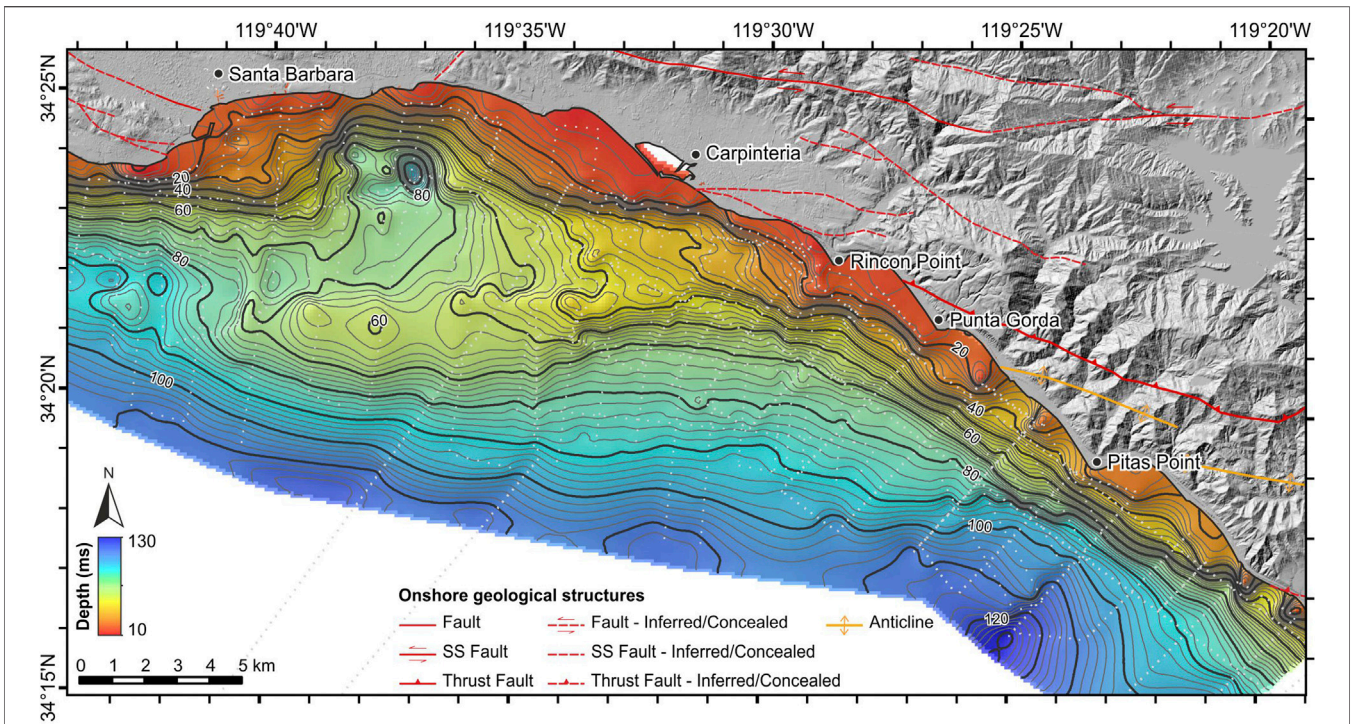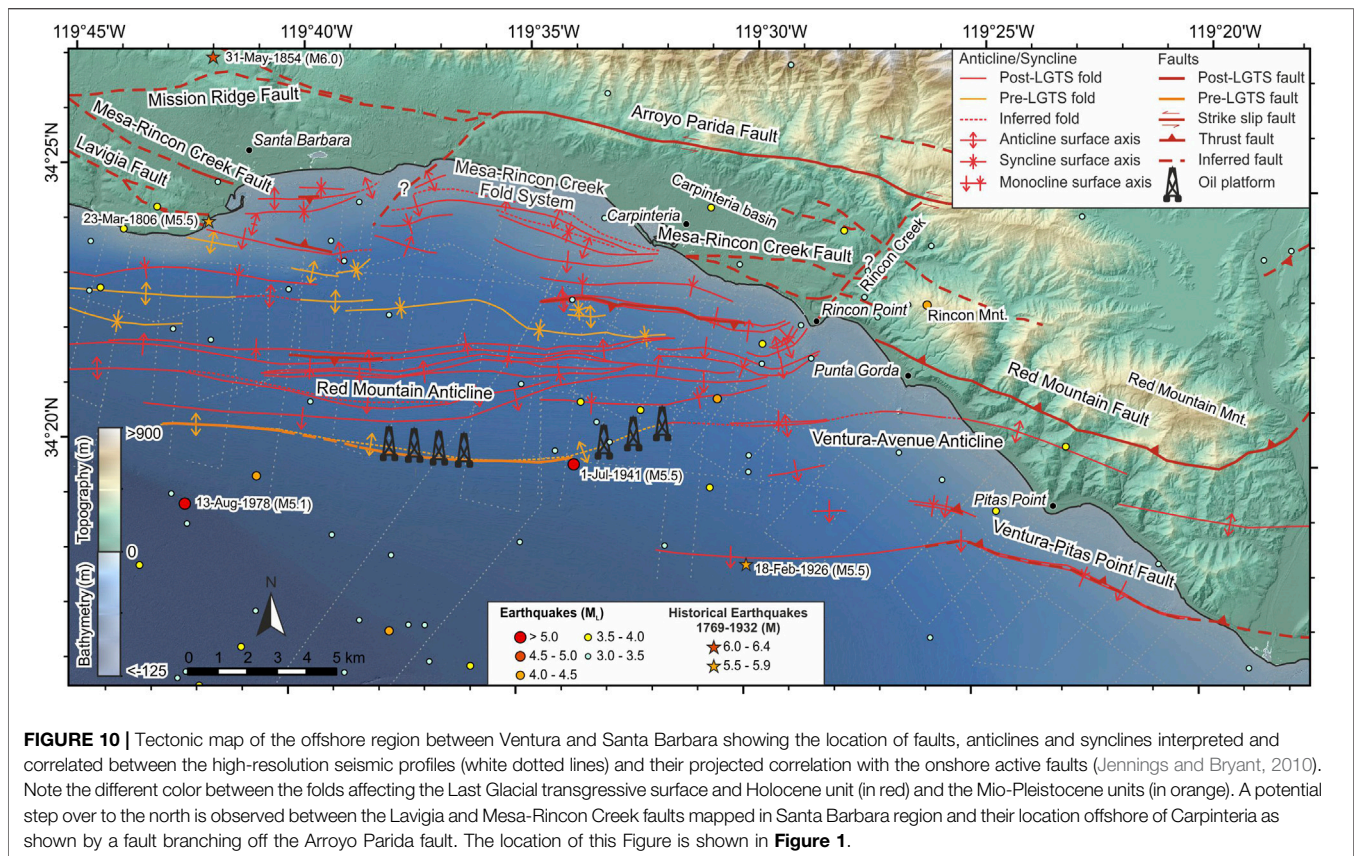
FIGURE 8 | Structural contour map of the Last Glacial transgressive surface (LGTS) in milliseconds two-way travel time (TWTT) for the offshore region. Control lines are shown by white dotted lines. Note the ENE-WSW elongated high starting at Rincon Point and the depression between it and the coastline, which corresponds to the Inner Santa Barbara Basin. Within this elongate depression, there is an abrupt short wavelength deepening (80 ms) of the LGTS. Main contour lines (black) are every 10 ms and secondary contour lines (gray) every 2 ms. For the interpolation, we used the Flex Gridding algorithm in IHS Kingdom software. Onshore shaded relief map shows the location of the main active faults (Jennings and Bryant, 2010). The location of this figure is shown in **Figure 1**.
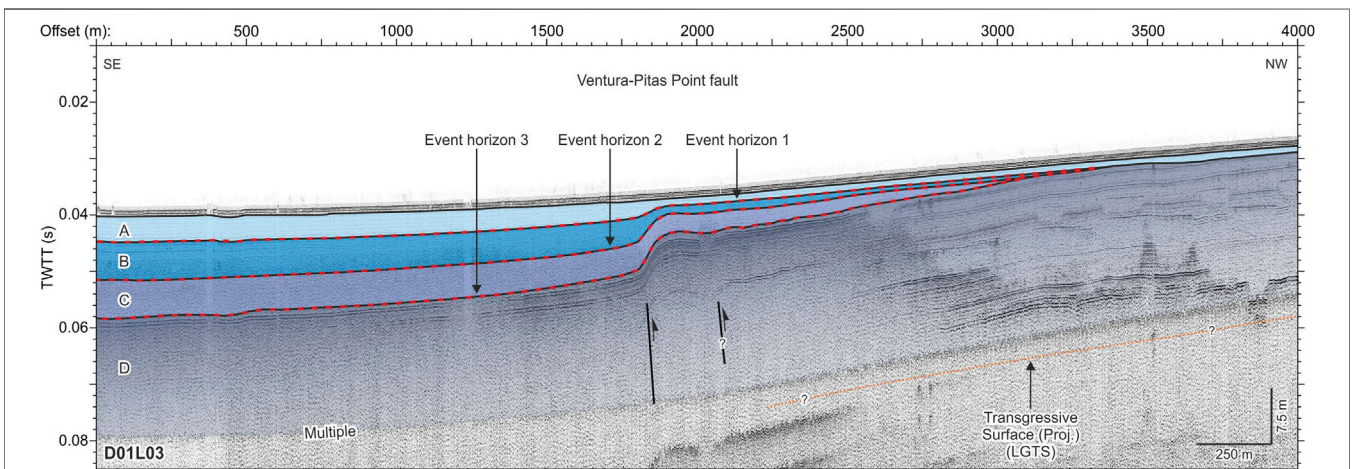
FIGURE 9 | Interpreted CHIRP profile D01L03 acquired across the Pitas point thrust fault. Different seismostratigraphic units (A–D) are identified based on stratal geometries. The red dashed lines identify horizons corresponding to different deformation events (i.e., inferred earthquakes). The LGTS (dashed orange line) is projected from the structural contour map as it is not well imaged as it is obscured by the multiple. The location of the profile is shown in **Figures 2**, **3**. Uninterpreted profile is provided in **Supplementary Figure S8**.

and **Supplementary Table S5**). In comparison, unit A, bounded by the seafloor and event horizon 1, is slightly thinner (0.004 s TWTT, approximately 3.4 m, at offset 750 m; **Supplementary Table S5**). Considering a constant sedimentation rate for the

Holocene, this may suggest that the time between events 1 and 2 and 2 and 3 was similar and that the time elapsed since the last event, event 1, would correspond approximately to two thirds of the time between the previous events.

FIGURE 10 | Tectonic map of the offshore region between Ventura and Santa Barbara showing the location of faults, anticlines and synclines interpreted and correlated between the high-resolution seismic profiles (white dotted lines) and their projected correlation with the onshore active faults (Jennings and Bryant, 2010). Note the different color between the folds affecting the Last Glacial transgressive surface and Holocene unit (in red) and the Mio-Pleistocene units (in orange). A potential step over to the north is observed between the Lavigia and Mesa-Rincon Creek faults mapped in Santa Barbara region and their location offshore of Carpinteria as shown by a fault branching off the Arroyo Parida fault. The location of this Figure is shown in **Figure 1**.
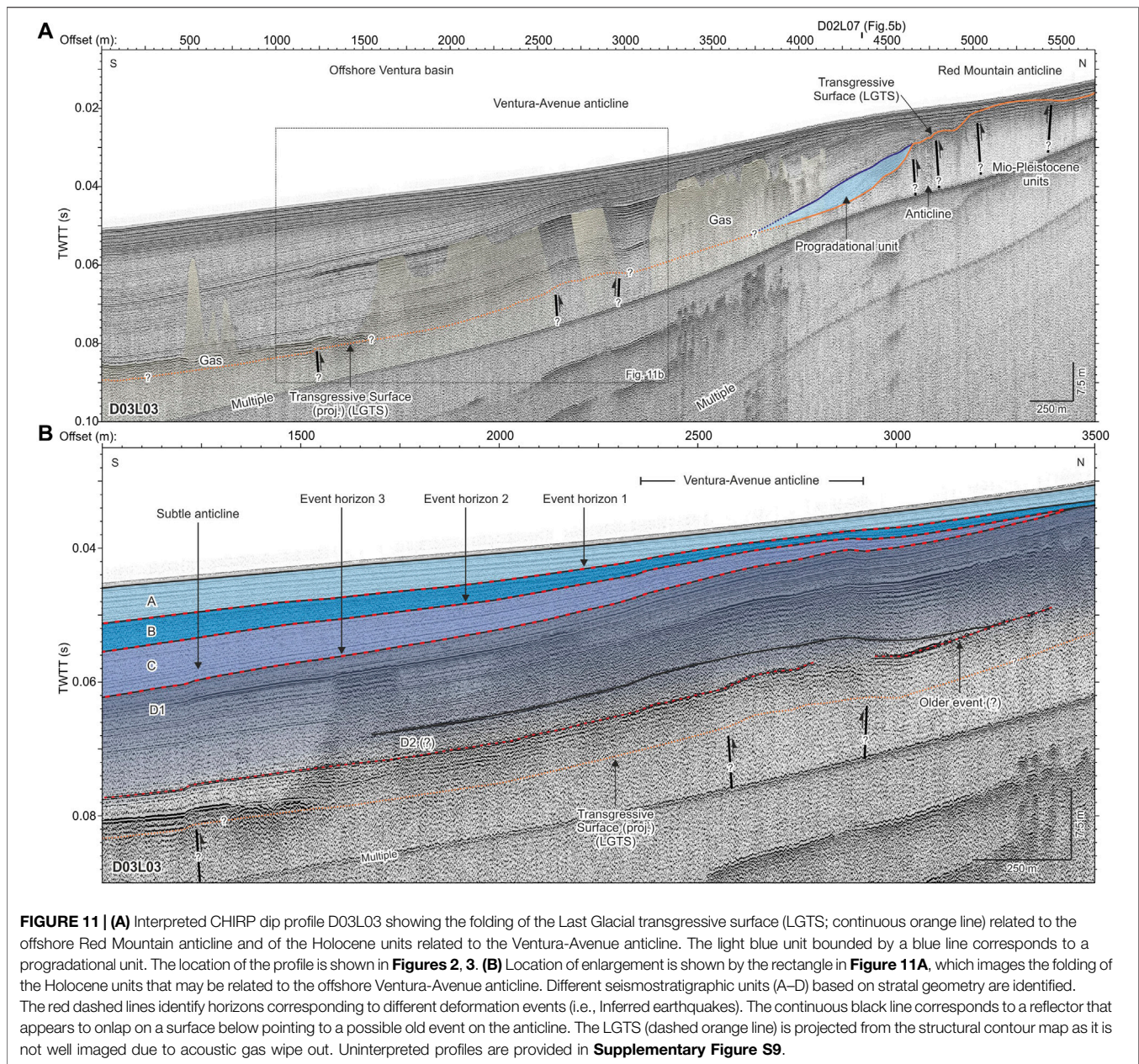
Ventura-Avenue Anticline Trend

In the CHIRP profiles located south of Rincon Point, we observe a gentle, low relief anticline about ~500 m long that folds Holocene sediments but not the seafloor (**Figure 11**). This anticline, which trends approximately E-W, becomes more difficult to identify towards the west and completely disappears at the longitude of Carpinteria. Farther west, we have identified an anticline with a similar trend, but with greater width and higher structural relief that folds the pre-LGTS sedimentary units and is offset by thrusts and backthrusts (**Figures 3**, **6A**, **7**). This anticline does not appear to deform the LGTS in this region. Several oil platforms are located along the axis of the anticlinal trend, which were used to correlate the structure between profiles where the structure was not well imaged in the seismic data. It appears that the anticline is a continuous structure, folding both the LGTS and the Holocene unit east of the longitude of Carpinteria, and just the pre-LGTS seismic-stratigraphic units to the west. The trend of this structure aligns with the onshore Ventura-Avenue anticline trend (also identified as the Rincon or Dos Cuadras anticline in the offshore), which is consistent with the nomenclature of other studies (Sorlien et al., 2000; Plesch et al., 2007; Hubbard et al., 2014; Sorlien and Nicholson, 2015; Johnson et al., 2017b; Levy et al., 2019). The anticline is observed for at least 27.5 km offshore (**Figure 10**); the portion where the anticline deforms the Holocene strata in this dataset extends offshore for approximately 10.3 km.

A seismic profile across the Ventura-Avenue anticline above the LGTS (**Figure 11B**) images three units below the seafloor with reflectors that onlap onto the upper reflector of the preceding unit forming different unconformities to the north and growth strata geometries to the south (**Figure 11B**). The units thin where they onlap the fold (**Figure 11A**). Units A and B exhibit slight thickening north of the Ventura-Avenue anticline and all three units thicken south of the axis of the anticline. Reflectors in units A, B, and C onlap the limbs of the anticline. A subtle monocline is observed south of the Ventura-Avenue anticline with folds at the base of unit C and the reflectors below (offset 1250 in **Figure 11B**). Three deformation events are imaged above the LGTS (events 1, 2 and 3; **Figure 11B**). Despite the prevalent acoustic gas wipe out in the region, there are some observations that may record an older event. For example, a possible unconformity is observed on the northern limb of the Ventura-Avenue anticline (offset 3150 and 0.054 s TWTT in **Figure 11B**).

To estimate the vertical uplift related to each event, we employed a similar approach used for the Ventura-Pitas Point fault. The vertical uplifts measured across the southern limb are in the range of 0.6–0.7, 1.1 and 0.6–0.7 m for events 1, 2 and 3, respectively (more information in **Supplementary Table S4**). Nevertheless, the identification of a monocline south of the anticline that has deformed event horizon 3 but no overlying reflectors (offset 1250 in **Figure 11B**) suggesting that the offshore
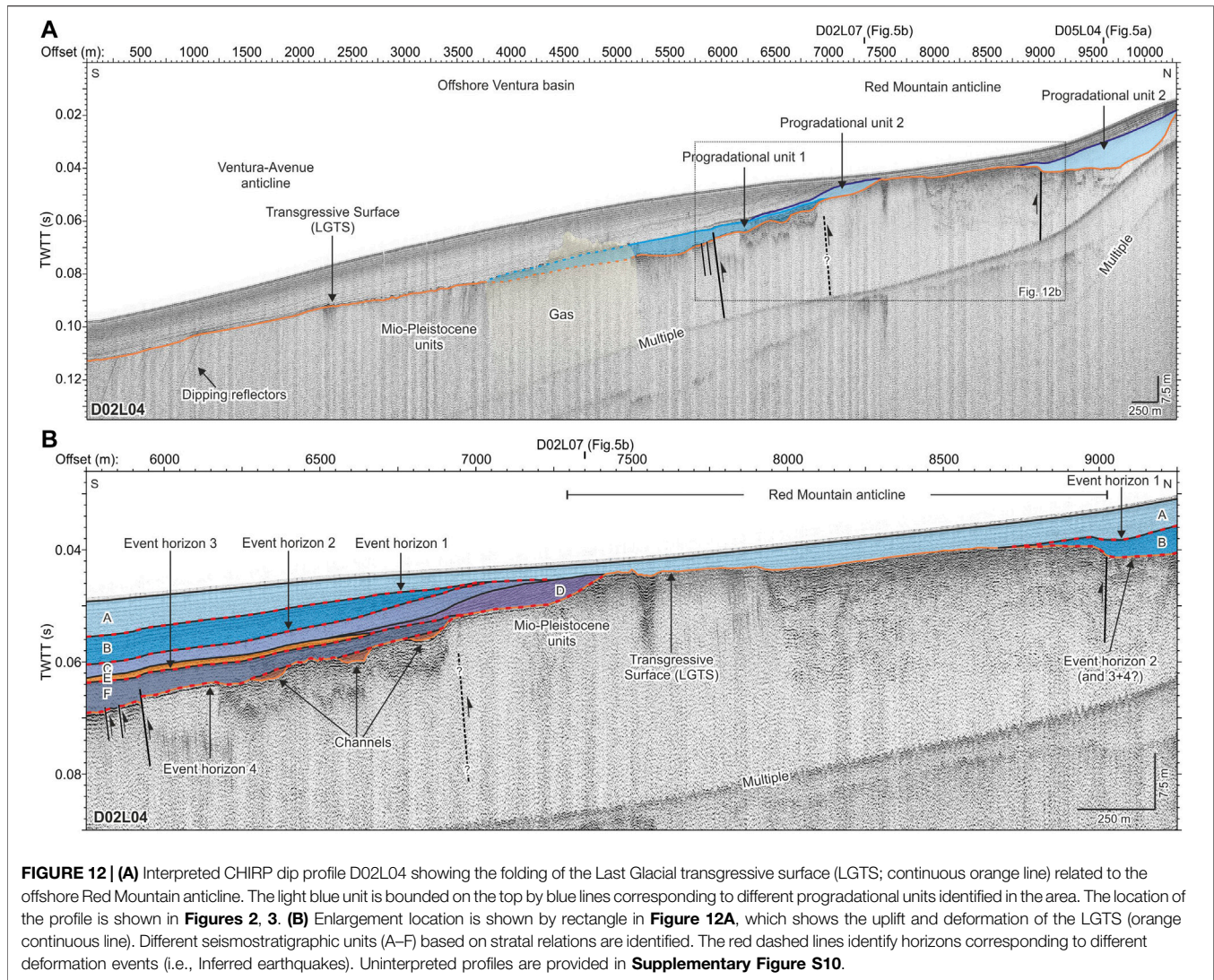
FIGURE 11 | (A) Interpreted CHIRP dip profile D03L03 showing the folding of the Last Glacial transgressive surface (LGTS; continuous orange line) related to the offshore Red Mountain anticline and of the Holocene units related to the Ventura-Avenue anticline. The light blue unit bounded by a blue line corresponds to a progradational unit. The location of the profile is shown in **Figures 2**, **3**. **(B)** Location of enlargement is shown by the rectangle in **Figure 11A**, which images the folding of the Holocene units that may be related to the offshore Ventura-Avenue anticline. Different seismostratigraphic units (A–D) based on stratal geometry are identified. The red dashed lines identify horizons corresponding to different deformation events (i.e., Inferred earthquakes). The continuous black line corresponds to a reflector that appears to onlap on a surface below pointing to a possible old event on the anticline. The LGTS (dashed orange line) is projected from the structural contour map as it is not well imaged due to acoustic gas wipe out. Uninterpreted profiles are provided in **Supplementary Figure S9**.

deformation may be split between different faults and folds. On the northern limb of the anticline, the measured vertical uplift values are ~0.7, ~0.9 and 0.6–0.7 m for the same events. It is important to not the similar uplift values on both limbs. Given that the CHIRP profiles crossing the anticline did not directly image the LGTS (**Figure 11**), we have not been able to estimate the vertical uplift rates. The thickness of units A, B and C, units above the different event horizons, is 0.005, 0.004 and 0.006 s TWTT, respectively (approximately 3.4, 2.6 and 4.4 m at offset 1500 m in **Figure 11B** and **Supplementary Table S5**).

Red Mountain Anticline

Analysis of the seismic profiles between Rincon Point and Santa Barbara reveals noticeable uplift and deformation of the LGTS

that forms an anticline 1–2.5 km wide, 6.7–29 m (0.009–0.039 s) of structural relief, and a total length of approximately 24.5 km (**Figures 3**, **6A**, **7**, **11A**, **12**, **13D**). This anticline trends E-W in the western part of the basin and becomes narrower as it progressively changes its trend to NNE-SSW to the east (**Figures 8**, **10**). In the central and western part of the basin, the southern limb of the anticline verges south showing an increase in slope when compared to the seafloor and forming a smooth fold. In contrast, a steeper monocline characterizes the northern limb, which diminishes to the east with an attendant change in trend of the main anticline (**Figures 3**, **6A**, **7**, **11A**, **12**, **13D**). Close to Rincon Point, there are a number of secondary monoclines that merge with the main structure (**Figure 10**). The northernmost one is associated with a fault that offsets the LGTS
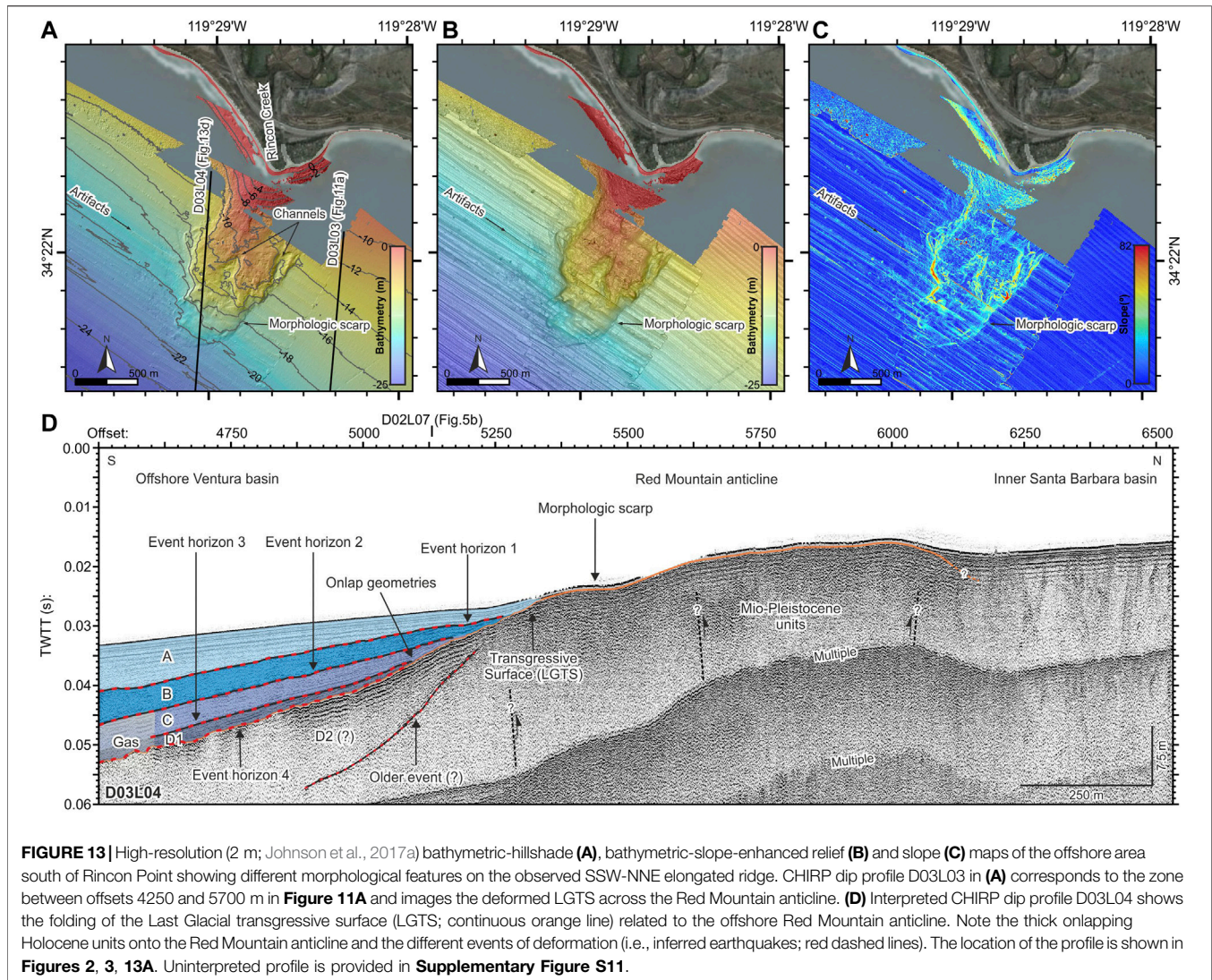
FIGURE 12 | (A) Interpreted CHIRP dip profile D02L04 showing the folding of the Last Glacial transgressive surface (LGTS; continuous orange line) related to the offshore Red Mountain anticline. The light blue unit is bounded on the top by blue lines corresponding to different progradational units identified in the area. The location of the profile is shown in **Figures 2, 3. (B)** Enlargement location is shown by rectangle in **Figure 12A**, which shows the uplift and deformation of the LGTS (orange continuous line). Different seismostratigraphic units (A–F) based on stratal relations are identified. The red dashed lines identify horizons corresponding to different deformation events (i.e., Inferred earthquakes). Uninterpreted profiles are provided in **Supplementary Figure S10**.

and, in some cases, reflectors at the base of the Holocene unit (**Figures 3, 12**). Hoyt (1976) using 3.5 kHz high-resolution profiles mapped this structure and named it the Red Mountain anticline as he associated it to the northern and southern branches of the Red Mountain fault. Analysis of CHIRP seismic profiles shows that the Holocene units mantling the LGTS to the north and south of this anticline are predominantly undeformed (**Figures 3, 7**). The vertical uplift between Santa Barbara and the zone where the anticline changes its trend is quite constant with the average uplift ranging between 12 and 13 m (more information in **Supplementary Table S6**). In contrast, the average vertical uplift increases to 20–22 m in the NNE-SSW trending section (**Figure 10** and **Supplementary Table S6**). Given that the mean depth of the LGTS to the south of the anticline in the western sector is 61.2 and 50.7 m in the eastern sector and considering the regional global sea level during the Last Glacial Maximum (Fairbanks, 1989; Stanford et al., 2011; Muhs et al., 2014; Reeder-Myers et al., 2015; Reynolds and Simms, 2015; Johnson et al., 2017b), the age for the formation

of the LGTS might range between 10.6–12.1 and 9.8–11.2 ka, for both sectors, respectively. This yields an estimation of the average uplift-rate for the western sector in the range of 1.0–1.2 mm/yr, and of 1.8–2.1 mm/yr for the eastern sector (**Supplementary Table S6**).

Based on stratal geometries observed in the CHIRP data, four deformation events are observed on the southern limb of the Red Mountain anticline in an expanded stratigraphic section. On the northern limb, only the two youngest events are recognized (**Figure 12B**). Events 1, 2 and 4 on the southern limb thin to the north by onlap. In addition, a fault offsetting the base of Unit F engenders a subtle fold observed in all the overlying event horizons (offset 5950 m in **Figure 12B**). Furthermore, a local growth strata is observed in unit A, which is not observed in the lower units. In contrast, event 3 corresponds to a marked change in stratal geometry between Unit F and Unit D. Unit F thins by onlap onto the southern Limb of the Red Mountain anticline. Conversely, Unit D is located up dip of Unit F and thins to the south by downlap onto both the LGTS and Unit F (**Figure 12B**).

FIGURE 13 | High-resolution (2 m; Johnson et al., 2017a) bathymetric-hillshade **(A)**, bathymetric-slope-enhanced relief **(B)** and slope **(C)** maps of the offshore area south of Rincon Point showing different morphological features on the observed SSW-NNE elongated ridge. CHIRP dip profile D03L03 in **(A)** corresponds to the zone between offsets 4250 and 5700 m in **Figure 11A** and images the deformed LGTS across the Red Mountain anticline. **(D)** Interpreted CHIRP dip profile D03L04 shows the folding of the Last Glacial transgressive surface (LGTS; continuous orange line) related to the offshore Red Mountain anticline. Note the thick onlapping Holocene units onto the Red Mountain anticline and the different events of deformation (i.e., inferred earthquakes; red dashed lines). The location of the profile is shown in **Figures 2**, **3**, **13A**. Uninterpreted profile is provided in **Supplementary Figure S11**.

Farther south, Unit E mantles Unit F and exhibits high amplitude reflectors at the base and top (**Supplementary Figure S10**).

The vertical uplift for each event on the north limb has been estimated using the same approach employed for previous structures. Accordingly, it ranges between 0.9 and 1.0 m for events 1 and 2 in the northern limb (more information in **Supplementary Table S4**). The lack of post-transgressive surface sediments mantling all the deformed area on the southern limb and being uplift by folding, precludes the approach used to constrain uplift rates along the northern limb of the Red Mountain anticline.

Mesa-Rincon Creek Fold System

Close to the shoreline between Carpenteria and Santa Barbara the CHIRP profiles show a wide (~2.5 km) deformation zone formed by a series of anticlines and synclines (**Figures 6**, **7**). A south verging anticline, 2–2.5 km wide and 14–26 m (0.019–0.035 s) of structural relief, bounds the area to the south and clearly folds and

uplifts the LGTS. Towards the north, there is a sequence of secondary synclines and anticlines verging slightly to the north that have less width and lower structural relief. Some of the secondary anticlines are offset by reverse faults dipping to the south, showing the relation of these folds to active faulting (fault at offset 10,150 **Figure 6**). In front of the main anticline, there is a localized structural depression spatially coincident to the region where the LGTS dips steeply to the north (**Figures 3A**, **4B**, **8**). The correlation of the different deformation zones between profiles shows that the fold system extends E-W for 16.3 km, following the morphology of the coastline (**Figure 10**). In addition, correlation of the secondary anticlines and synclines suggests that there is a step-over between structures close to Santa Barbara versus structures east of the branch splaying off the Arroyo Parida fault (**Figure 10**). Furthermore, the syncline-anticline system to the north of the Lavigia fault/anticline may connect with the Mesa-Rincon Creek fault mapped in Santa Barbara to the west and to a NE-SW trending fault that branches off the Arroyo Parida fault in between Carpinteria and Santa Barbara

(**Figure 10**). The USGS sparker profile in **Figure 4A** is located to the west of the step over and the CHIRP profile in **Figure 4B** is to the east of it (**Figure 2**). The Lavigia fault imaged in **Figure 4A** (offset 3000) dies away to the east and the deformation across the step-over shifts to the north as observed in **Figure 4B** (offset 8750). Evidence for the step is also revealed in the fault map (**Figure 10**). Considering the onshore extension of the Lavigia (~8.7 km) and the Mesa-Rincon Creek (~7.5 km) faults, the total length of the system would be approximately 32.5 km. Vertical uplift and uplift-rates for the LGTS related to the frontal anticline have been estimated. Between Santa Barbara and west of Carpinteria, the average vertical uplift ranges from 24 to 26 m with an uplift-rate between 2.0 and 2.4 mm/yr, whereas to the east the uplift diminishes to 15–16 m with an uplift rate of 1.4–1.5 mm/yr (more information in **Supplementary Table S6**).

Unconformities associated with the deformation imaged in the CHIRP profiles delineates four Holocene uplift events related to the Mesa-Rincon Creek frontal anticline (**Figure 4B**), to the east of the step over, and four prominent events in the syncline-anticline system (**Figure 6B**), north of the Lavigia fault and west of the step over. In the Mesa-Rincon Creek frontal anticline, the evidence for event 1 is the recognition of onlap and downlap relationships of unit A onto unit B. The identification of events 2 and 3 is based on the observation of a seismostratigraphic succession between aggradation (units G and D) and progradation (units E and C) units (**Figure 4B**). Event 4 is based on the folding and deformation of the LGTS and attendant thickening of unit H towards the north. The vertical uplift for events 1 and 2 range between 10.6–11.3 m and between 3.9–4.2 m, respectively (more information in **Supplementary Table S4**). In the cases of event 3 and 4, it is not possible to estimate the uplift because the basal unconformity is obscured by the seafloor multiple (**Figure 4B**).

Unconformities and unit geometries observed in the syncline-anticline system (**Figure 6B**) reveal four uplift deformation events, which are consistent with the events determined for the Mesa-Rincon Creek frontal anticline (**Figure 4B**). Evidence for Event 1 is based on unit A thinning by downlap and onlap onto units B and C (**Figure 6B**). Events 2, 3 and 4 at the base of units B, E, and H in the syncline-anticline system are based on observed onlaps onto the event horizons. The LGTS is folded and faulted in the region. A reverse fault offsets both the bases of Unit G and F (offset 10,200 in **Figure 6B**). Farther south, another reverse fault offsets the base of Unit H and G (offset 9,500 in **Figure 6B**). Minor deformation may be observed at the base of Unit F and D; however, the evidence is not as compelling as for the other events (e.g., events 1–4).

The vertical uplift in the syncline-anticline system (**Figure 6B**) has been measured using two different approaches. For event 1, we have assumed that the top of unit B on each side of the anticline would follow the far field slope and, then, the difference in height would correspond to the uplift related to the event. Accordingly, it would range between 2.2 and 2.3 m. For event 3, we have considered that the event horizon would be flat, even it may slightly dip to the south, before the occurrence of the event. Then, the difference in height between the anticline and syncline axis would be the result of the cumulative uplift of this event and
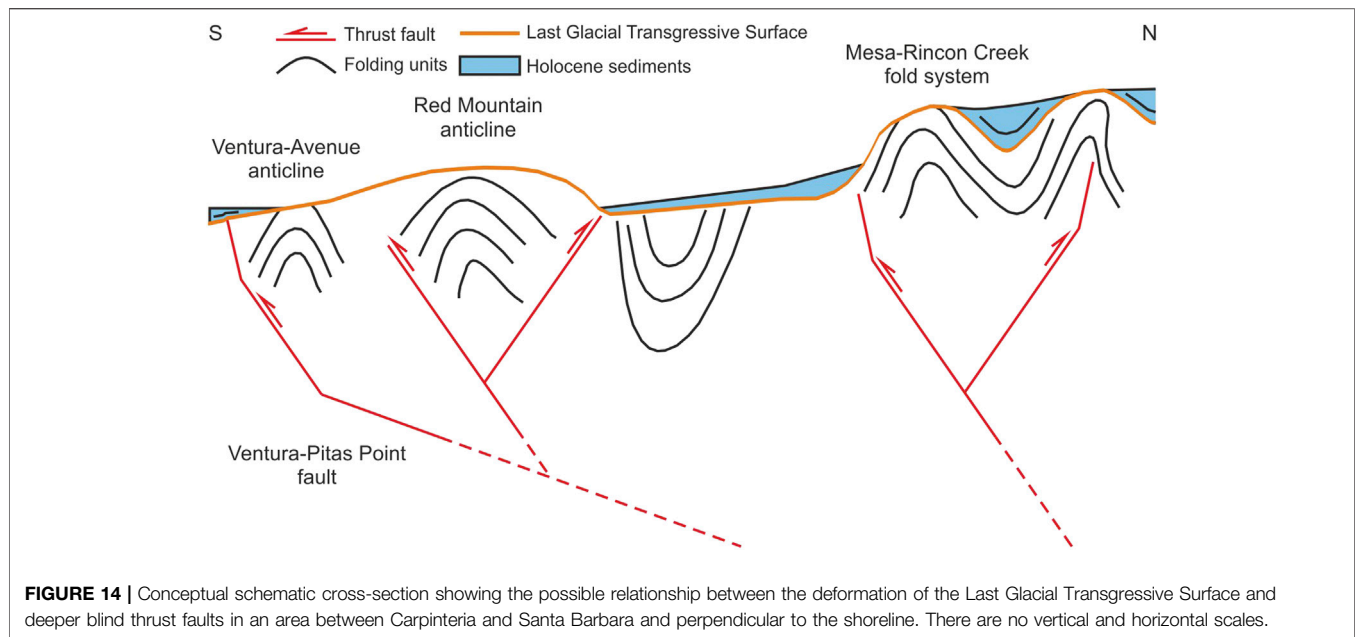
the more recent events (1 and 2), assuming no erosion. The obtained cumulative uplift for events 2 and 3 ranges between 9.0 and 9.6 m. Thus, these two events appear to have an average vertical uplift of ~4.6 m. Given that the CHIRP profiles crossing the syncline-anticline system did not continuously image the LGTS (**Figure 6**), we have not been able to estimate the vertical uplift rates.

DISCUSSION

Onshore-Offshore Structural Correlations

The new offshore geophysical data show that the Ventura-Pitas Point fault and the Ventura-Avenue anticline trend continue offshore (**Figure 10**). The Ventura-Pitas point fault can be mapped offshore for 19 km and the Ventura-Avenue anticline trend for 27.5 km. Previous studies, however, suggest that the system may extend west to the longitude of Point Conception for a total length of ~110 km (Sorlien et al., 2000; Sorlien and Nicholson, 2015; Johnson et al., 2017b). Moving west away from the coastline, the monocline associated with the Ventura-Pitas Point fault imaged in the CHIRP seismic data becomes more subdued with deformation of only the deeper Holocene reflectors (**Supplementary Figure S3**). In the case of the Ventura-Avenue anticline trend, the seismic profiles show that this structure is folding the LGTS and the Holocene units approximately 10.3 km westward from the coastline to a longitude equivalent to Carpinteria (**Figure 10**). West of Carpinteria, neither the LGTS nor the Holocene units appear to be deformed (**Figure 3**). The lack of evidence of shallow deformation associated with these structures in the west portion of the study region could be related to a subtle tilting of the southern wide limb of the anticline system due to the deepening of the thrust fault tip from east to west (Hubbard et al., 2014; Sorlien and Nicholson, 2015; Johnson et al., 2017b; Levy et al., 2019). Nevertheless, our new geophysical observations that define the change in the recency of deformation from east to west may suggest that these structures west of Carpinteria are accommodating less strain and becoming less active during this time period. In light of the new interpretations, the sections of both the Ventura Pitas Point and the Ventura Avenue anticlines that show clear deformation of the seismostratigraphic units above the LGTS have a total length of ~35 km when combined with their onshore-offshore extension.

The Mesa-Rincon Creek fold system has been identified onshore in Santa Barbara and from Carpinteria east to Rincon Creek (Dibblee, 1982; Jackson and Yeats, 1982; Olson, 1983; Jennings and Bryant, 2010; Gurrola et al., 2014) (**Figure 10**). The comparison between the fault and fold systems mapped onshore and offshore allows us to correlate the structures across the area. In the Carpinteria area, the basis for the correlation is that the identified offshore fold system ends close to the coastline where the Mesa-Rincon Creek fault is observed and both have similar trends. In Santa Barbara, two anticlines almost reaching the coastline may correlate with the Lavigia fault to the south, and farther north, the Mesa-Rincon Creek fault. The Lavigia fault

FIGURE 14 | Conceptual schematic cross-section showing the possible relationship between the deformation of the Last Glacial Transgressive Surface and deeper blind thrust faults in an area between Carpinteria and Santa Barbara and perpendicular to the shoreline. There are no vertical and horizontal scales.

appears to continue offshore for ~6 km. A step-over between the fold systems appears to be delineated by a NE-SW trending fault splaying off the Arroyo Parida fault (**Figure 10**). Close to this step-over, the frontal anticline on the eastern section bends and trends to the SW and the deformation steps northward (**Figure 4B**). The eastern extent and trend of the Lavigia fault also appears to be controlled by the step over, with the eastern limit of the deformation imaged in the sparker data showing much less structural relief than close to the coast line (**Figures 4A, 6A**) and a change in strike from WNW to the ENE. Such opposite heading directions at both sides of the step-over could indicate some kinematic control and suggests the presence of a left-lateral tear-fault that would accommodate differential movement on the NE-SW trending fault that branches off the Arroyo Parida fault (**Figure 10**).

The Red Mountain fault has been previously extended towards the offshore areas following the trend of an offshore mapped anticline (Hoyt, 1976; Jackson, 1981; Plesch et al., 2007; Hubbard et al., 2014; Sorlien and Nicholson, 2015; Johnson et al., 2017b) identified as the Red Mountain anticline (Hoyt, 1976). The analysis of the new high-resolution dataset offshore, even in areas with limited imaging; however, suggests that there is no lateral continuity between the onshore fault and the offshores anticline (**Figure 10**). Continuing east, the Red Mountain anticline progressively bends towards the NE with its width decreasing where it approaches the coastline (**Figure 10**). It has bathymetric expression in shallow water as a NNE-SSW elongated ridge offshore Rincon Point (**Figure 14**). In addition, this alignment appears to act as a structural and drainage boundary. Onshore, the Rincon Creek separates the Rincon Mountain and Red Mountain topographic high zones in the east, which progressively lowers from east to west, from the Carpinteria basin to the west (**Figure 10**). Offshore, the Red Mountain anticline separates two Holocene sedimentary basins,

with the Offshore Ventura Basin to the southeast and the Inner Santa Barbara Basin to the northwest (**Figure 3**).

In shallow water where the Red Mountain anticline comes onshore, it is delineated by the previously mentioned elongated ridge with steep NW and SE lateral margins (**Figure 13**). The top of the ridge is an almost planar surface, possibly a marine terrace, that gently dips to the SW. Two channel features are observed; however, the main channel is not connected to the current onshore drainage. A subdued north facing E-W trending morphological scarp is present along the southern portion of the ridge (**Figures 13A–C**). Johnson et al. (2017b) described this elongated ridge as a lobate boulder delta related to the Rincon Creek and correlated the subdued morphological scarp with the offshore trace of the north dipping Red Mountain thrust. The CHIRP profiles show that the top of this ridge corresponds to the deformed LGTS that exposes transgressive lag deposits at the seafloor (**Figure 13D**). Furthermore, on both sides of the ridge, the Holocene unit onlaps onto the LGTS. Within the Holocene unit, there are different onlapping subunits (i.e., interpreted as event horizons) that record the uplift and deformation of the anticline (**Figures 11A, 13D**). Accordingly, we interpreted this ridge as an uplifted area of the Miocene-Pleistocene units and transgressive lag deposits associated with the Red Mountain anticline. Finally, Johnson et al. (2017b) interpret the northward facing morphological scarp as evidence for the north dipping Red Mountain thrust fault. If correct, the scarp should be south facing for a northward dipping thrust fault, not northward facing, although it may represent a back-thrust scarp and not the main Red Mountain fault. Furthermore, if the scarp records thrust activity during the Holocene, it should also offset the adjacent Holocene sediments in the Ventura basin. There is no evidence of a similar scarp in the bathymetry, or a fault offsetting the Holocene unit towards the east (**Figures 11A, 13**). The evidence ascribing this scarp to an active north dipping thrust fault is not compelling.

In contrast with the fault models that extend the Red Mountain fault offshore (Hoyt, 1976; Plesch et al., 2007; Hubbard et al., 2014; Sorlien and Nicholson, 2015; Johnson et al., 2017b), we suggest that the Red Mountain anticline offshore and the Red Mountain fault onshore are independent structures but with the same trend. Based on the offshore and onshore observations, it appears there may be a tear fault or a lateral ramp aligned with Rincon Creek (**Figure 11**). This creek has two characteristics that may indicate that it is tectonically controlled. First, is a very rectilinear drainage when compared with the other creeks in the area (i.e., the creeks across the Rincon and Red Mountain mountains). Second, as previously discussed, there is a clear boundary along this creek with a basin area to the NW (i.e., the Carpinteria basin) and a topographic elevated area to the SE, with the Rincon and Red mountains (**Figure 11**). Following the creek, this fault could splay off the Arroyo Parida fault to the north; this eastern branch has a similar trend to the western branch (tear fault) off the Arroyo Parida fault. The onshore section of the fault might be predominantly strike-slip with some dip-slip component, which considering its trend, is consistent with the GPS velocity vectors near Rincon Creek (Marshall et al., 2013) (**Figure 1**). Finally, this structural relationship is similar to that observed in the Mesa-Rincon Creek fold system to the west and to other fault terminations along the Western Transverse Ranges, including the eastern termination of the Red Mountain fault onshore, the central part of the San Cayetano fault as well as along the Santa Susana fault (Dibblee, 1982; Rockwell, 1988; Yeats et al., 1994; Levy et al., 2019).

Migration of Active Deformation and Shortening Rates

Map restoration of folded strata for the past 6 Ma (Sorlien et al., 2000) and 1.5 Ma (Sorlien and Nicholson, 2015) and geodetic data and inversion of horizontal GPS velocities (Marshall et al., 2013) carried out in the Western Transverse Ranges show an east to west decrease of the contractional deformation across the Ventura Basin and Santa Barbara Channel. Interpretation of CHIRP profiles also reveal that the offshore deformation affecting the LGTS diminishes westward. Nevertheless, the observed decrease in deformation coincides geographically with an increase along other structures farther north closer to the shoreline. For example, the Ventura-Avenue anticline extends from the coastline between Punta Gorda and Pitas Point to the west of Santa Barbara. Folding the LGTS and the mantling Holocene units is observed between Pitas Point and Carpinteria (**Figures 11**, **12A**). In contrast, west of Carpinteria deformation of the LGTS or the overlying Holocene sediments is not observed (orange segment, **Figure 10**); however, the underlying Mio-Pleistocene units in this region are clearly deformed (**Figure 3**). In this region, the Ventura-Avenue anticline appears to have been less active during the Holocene, or at least post-transgression (**Figures 3**, **6A**, **7**). This potential change in activity occurs in the zone where the Ventura-Avenue anticline runs parallel and approaches to the Red Mountain anticline, and where the Red Mountain anticline exhibits

Holocene deformation (**Figures 8**, **10**). A similar pattern of deformation is observed between the Red Mountain anticline and the Mesa-Rincon Creek fold system. The uplift rates estimated along the northern limb of the Red Mountain anticline since the formation of the LGTS (~11 ka) show that these rates slightly diminished towards the west. Close to Rincon Point the uplift rates range between 1.8 and 2.1 mm/yr, while from Carpinteria to the west the rates diminish to 1.0–1.2 mm/yr (**Supplementary Table S6**). In contrast, for the same period of time, the uplift rates obtained for the frontal anticline of the Mesa-Rincon Creek fold system increase from Carpinteria towards the west. Close to Carpinteria the rates range between 1.4 and 1.5 mm/ka and towards Santa Barbara the rates rapidly increase up to 2.0–2.4 mm/yr (**Supplementary Table S6**). The comparison between the rates obtained for both structures show that around Carpinteria the rates in the Red Mountain anticline diminish to the west, whereas the rates on the Mesa-Rincon Creek fold system increase. Taking into account the uncertainties in the data used to estimate the vertical uplift rates, it is reasonable to consider that the maximum rates in both structures are quite similar and around 2.0 mm/yr.

Rockwell et al. (2016) studied different marine terraces uplifted by activity along the Ventura-Avenue anticline between Punta Gorda and Pitas Point (**Figure 2**). They obtained a vertical uplift rate of 5.75 mm/yr for the last 6.7 ka. Between Santa Barbara and Goleta (**Figure 1**), Gurrola et al. (2014) analyzed a set of marine terraces and obtained a vertical uplift rate between 1.1 and 1.2 mm/yr for the last 58–70 ka in Santa Barbara and between 1.8 and 2.0 for the last 48 ka east of Goleta. The authors suggest that these rates are the result of displacement and folding associated with different structures corresponding to the Mesa-Rincon Creek fold system. Comparing the uplift rates, we have obtained for the Red Mountain anticline and the Mesa-Rincon Creek fold system with the results for the Ventura-Avenue anticline, it is evident that for a similar time span the uplift rates obtained from the terraces are almost three times larger. Nevertheless, inversion of horizontal geodetic data for the whole Western Transverse Ranges show that the contraction rates along the southernmost Ventura Basin decrease both to the west and east (Marshall et al., 2013). Accordingly, the uplift rates for the structures west of Ventura may be lower, thus possibly explaining the lower rates obtained for the Red Mountain anticline and the Mesa-Rincon Creek fold system. Otherwise, the vertical uplift rates reported in Santa Barbara are approximately half of the rates obtained for the frontal anticline of the Mesa-Rincon Creek fold system. The approach used to calculate the vertical uplift rates relies on the age obtained for the LGTS at the different locations. This age is estimated measuring the depth of the LGTS below the present sea level and compared with different sea level curves for the Holocene (Fairbanks, 1989; Stanford et al., 2011; Muhs et al., 2014; Reeder-Myers et al., 2015; Reynolds and Simms, 2015; Johnson et al., 2017b). Although this approach provides a maximum and minimum age for the LGTS at each location, the estimated ages have much more uncertainty than the ages obtained for the marine terraces using numerical dates (i.e., OSL,

Uranium series or Radiocarbon; Gurrola et al., 2014). Accordingly, the rates obtained from the analysis of the marine terrace may be more reliable. Nevertheless, the time span covered offshore is around 10 ka, whereas onshore extends up to 70 ka. Change in the slip rate for different time ranges has been shown for the San Cayetano South fault (**Figure 1**), with a slip rate of 1.9 mm/yr since ~19–7 ka and of 1.3 mm/yr for the last ~7 ka (Hughes et al., 2018). Accordingly, it may be possible that the vertical uplift calculated onshore Santa Barbara may be an average of different tectonic moments with the structures accommodating distinct deformation rates through time. In addition, uplift rates estimated east of Goleta are quite similar to those calculated offshore, showing that despite some discrepancies, the offshore uplift rates are in the range of the rates obtained onshore between Santa Barbara and Goleta.

The observations suggest that during the Holocene and from east to west, the structures accommodating the maximum surface deformation are located farther north closer to the coastline and exhibit a right-stepping pattern from east to west, consistent with a left-lateral component of shear. Between Ventura and Rincon Point, the main Holocene active structures appear to be the Ventura-Pitas Point fault and the Ventura-Avenue anticline, with minor Pleistocene activity associated with the Red Mountain fault (Lindvall et al., 2002). The Red Mountain anticline and the Mesa-Rincon Creek fold system appear to accommodate more of the deformation between Rincon Point and Santa Barbara. Nevertheless, west of Carpinteria the main deformation appears to be accommodated by the Mesa-Rincon Creek fold and back-thrust system. Two different hypothesis could explain the observed change in activity across the fold system. One possibility may be related to the tilting of the southernwide limb (5 km) of the Ventura-Avenue anticline to the west of Rincon Point (Sorlien and Nicholson, 2015), which would be difficult to observe in the LGTS or Holocene deposits due to the very low increment in titling (~0.23˚ considering 20 m of vertical uplift in a 5 km wide limb). The other possibility would imply an out-of-sequence propagation of the deformation in the thrust system during the Holocene on the offshore Western Transverse Ranges. As such, it would limit or diminish the activity on the frontal structures of the system to re-activate or transfer the main activity to faults and folds closer to the hinterland towards the west. In this alternative hypothesis, with the understanding that the Ventura-Pitas Point fault and the Ventura-Avenue anticline are the frontal structures of the system with observed Holocene activity onshore and offshore, the question then arises, why does it become apparently inactive during the Holocene from Rincon Point to the west? The only change in the system during this last 10 ka has been the rise of sea level. Different studies have shown that large changes in water levels can affect the stress field locally and regionally and favor or prevent fault slip (Luttrell and Sandwell, 2010; Brothers et al., 2011; Neves et al., 2015). Luttrell and Sandwell (2010) calculate the eustatic ocean loading at the Cascadia Subduction System and conclude that when sea level is high the system would preferably fail in deeper segments below the continent, whereas in times of lower sea level it would preferable rupture the shallower offshore portions of the fault zone. The implications for the offshore

Transverse Ranges is that rupture of faults closer to the continent (Red Mountain anticline) would occur during sea level highstands. Conversely, rupture on the offshore faults (Ventura-Pitas Point system) would be more likely during sea level lowstands, which may explain the low deformation along the frontal structures during the Holocene. The accumulated stress would be released along structures in the hinterland systems, such as the Red Mountain anticline. The same mechanism may explain the larger deformation in the Mesa-Rincon Creek fold systems as compared to the Red Mountain anticline west of Carpinteria (**Figure 6**).

Based on the uplift observed in the Red Mountain anticline and to the frontal anticline of the Mesa-Rincon Creek fold system, we have estimated the vertical uplift rates for the Holocene, which are roughly consistent with uplift rates calculated from marine terraces. Different geological cross-sections across the Western Transverse Ranges relate the anticlines to different blind-thrusts (Yeats et al., 1987; Yerkes et al., 1987; Rockwell, 1988; Rockwell et al., 1988; Yeats et al., 1988; Shaw and Suppe, 1994; Huftile and Yeats, 1995; Sorlien et al., 2000; Azor et al., 2002; Plesch et al., 2007; Hubbard et al., 2014; Levy et al., 2019). Considering the vertical uplift rates (~2 mm/yr) and knowing the dip of the blind-thrusts, it is possible to calculate the net slip rate and the shortening rate on the faults. Structural forward modelling of the Western Transverse Ranges using Trishear show that the blind-thrust faults related to the Red Mountain anticline and to the frontal anticline of the Mesa-Rincon Creek fold system may dip between 50˚ and 60˚ (Levy et al., 2019). Accordingly, the net slip rate may range between 2.3 and 2.6 mm/yr and a shortening rate between 1.2 and 1.7 mm/yr. Geodetic data reveal north-south convergence across the Ventura Basin at ~7 10 mm/yr (Donnellan et al., 1993a, 1993b; Hager et al., 1999; Marshall et al., 2013). Comparing the calculated shortening rate to the geodetic rate suggests that the anticline systems in the Offshore Ventura and the Inner Santa Barbara basins might be accommodating between 12 and 24% of the convergence in this area of the Western Transverse Ranges.

Inferring the Deep Structure From Post-LGTS Deformation

The CHIRP profiles image the surficial stratigraphy (top tens of meters) with submeter vertical resolution. The majority of the faults in the basin are blind thrusts with their fault tips hundreds of meters below the seafloor (Yerkes et al., 1987; Namson and Davis, 1988; Shaw and Suppe, 1994; Hubbard et al., 2014; Sorlien and Nicholson, 2015; Johnson et al., 2017b; Levy et al., 2019). As a result, the CHIRP profiles do not image most fault offsets in the region. Nevertheless, they show the deformation and folding of the LGTS and Holocene unit that provides constraints on the geometry of the deep blind thrusts. Based on this information, we propose a geological model of the deep structure based on the observed surficial deformation in the offshore Ventura and Inner Santa Barbara basins (**Figure 14**). Levy et al. (2019) have published a set of geological cross-sections across the Western Transverse Ranges, some of them between Ventura and Santa Barbara. These cross-sections show good agreement with our

observations and conceptual model, showing the importance of analyzing the surface deformation to provide additional constraints on the deep structure.

The surface deformation along the identified Ventura-Pitas Point fault and the Ventura-Avenue anticline appears to be related to the activity on the southernmost main thrust of the system. Interpretation of the seismic profiles show that close to Ventura, the Ventura-Pitas Point fault is a narrow, low structural relief monocline verging to the south with a possible high-angle, reverse fault close to the seafloor (**Figure 9**). A low relief anticline that exhibits approximately hectometer wavelength 650 m wide zone of Holocene deformation is interpreted as the surficial expression of the Ventura Avenue anticline (**Figure 11**) with attendant folding of the Mio-Pleistocene units below the LGTS to the west (**Figures 6A**, **7**). Such observations suggest that both structures may be related to a high-angle north-dipping thrust fault close to the seafloor that generates the Ventura-Pitas Point fold and the Ventura Avenue anticline. This fault has been identified as the Ventura-Pitas Point fault and its dip is interpreted to shoal at depth to account for the regional rate of uplift (Levy et al., 2019). Our interpretation is in agreement with previous structural models based on seismic and well data (e.g., Namson and Davis, 1988; Shaw and Suppe, 1994; Hubbard et al., 2014; Sorlien and Nicholson, 2015; Johnson et al., 2017b) and with models obtained by Trishear forward structural modelling (Levy et al., 2019).

To the north of the Ventura-Pitas Point fault and in the center of the offshore basin, there is the Red Mountain anticline, with kilometer-scale width and low to moderate structural relief (**Figures 3**, **6A**, **7**). In the central part of the basin, the anticline has a gentle slope on the southern limb and a steeper slope on the northern limb, with some local uplift along the axis. This local deformation may be related to a shallow back thrust fault dipping to the south and branching into the main blind thrust that dips to the north. It is important to note in our interpretation, the main offshore thrust may not correlate with the onshore Red Mountain fault, as it appears to die away to the east into a tear fault (**Figures 10, 14**). The main blind thrust causing the offshore Red Mountain anticline could be a northern branch off the detachment associated with the Ventura-Pitas Point fault. Such a geometry is consistent with the hypothesis that the deformation is transferred from the southern to northern structures moving west in the region. In comparison with Levy et al. (2019) cross-sections (4 and 5 in their **Figures 4**, **10**). They identify the faults bounding the Red Mountain anticline as being the Red Mountain fault and associated backthrusts, In our preferred interpretation, we propose that west of Rincon Point the thrust system would not correspond to the onshore Red Mountain fault.

The most northern and western structure in the offshore basin is a wide deformation zone that corresponds to the Mesa-Rincon Creek fold system, composed of a series of anticlines and synclines (**Figures 6A**, **7**). The largest structure corresponds to the southern anticline that exhibits a prominent southern limb with kilometer-scale width and large structural relief. Towards the north, there is a syncline-anticline sequence with a shorter width, verging slightly to the north. This deformation is in shallow water and is not imaged by the deep seismic data

(Sorlien and Nicholson, 2015). In addition, there is a local depocenter where the LGTS dips steeply to the north and localized in front of the main anticline east of the proposed left-lateral tear-fault (**Figures 3A**, **4B**, **8**). In our conceptual model (**Figure 14**), the large anticline and the local depocenter may be related to a blind thrust dipping to the north, similar to Ventura Pitas Point fault, with a steeper dip close to the seafloor to explain the large uplift with the short width of deformation compared with the Red Mountain anticline (**Figure 14**). To the north, a back-thrust that dips steeply to the south would explain the northern anticline (**Figures 6B**, **13**). This model agrees with geological cross-section and trishear forward modelling by Levy et al. (2019) in Santa Barbara. In addition, they show that the main thrust fault may branch with the Ventura-Pitas Point fault at depth. The main difference with our conceptual model is that the thrust identified as the Red Mountain fault in their cross-section (5 in their **Figures 4**, **10**) would represent the Mesa-Rincon Creek fold system. At depth, the connection of the northward dipping thrust of the Mesa-Rincon Creek fold system to a regional detachment may explain the apparent jump of the deformation from the Red Mountain anticline to the Mesa-Rincon Creek fold system towards the west.

Correlation of the Deformation Events Between Onshore-offshore

Two onshore paleoseismological studies provide important constraints on the most recent earthquake and the recurrence interval, one focused on the Ventura-Pitas Point fault (McAuliffe et al., 2015) and the other on the Ventura-Avenue anticline (Rockwell et al., 2016). McAuliffe et al. (2015) analyzed continuously cored boreholes and cone penetrometer tests (CPTs), high-resolution seismic-reflection data, and luminescence (IRSL) and ^{14}C dates from Holocene strata across the Ventura-Pitas Point fault in the city of Ventura. Evidence for at least two deformation events is reported (**Figure 15**). The youngest event is interpreted to have occurred between 235 and 805 yr ago and produced a vertical uplift between 6 and 6.5 m. The older event took place between 4065 and 4665 yr ago with a maximum vertical uplift between 4.5 and 5.2 m. The deformation observed for the older event may be recording two events that occurred close together in time, as they observed evidence for different bed dips in the successive units. The older of the two events might have occurred between 4165 and 4590 yr ago. As mentioned, the CHIRP profiles show evidence of at least three Holocene deformation uplift events associated with the Ventura-Pitas Point fault (**Figure 9**). The last two offshore events are characterized by vertical uplifts that are approximately half of those estimated for the onshore deformation. Two different processes could explain this onshore-offshore uplift difference. On one hand, the fault system would accommodate less deformation towards the west into the offshore, an observation that is consistent with the progressive decrease in structural relief of the monocline observed in the seismic dataset towards the west (**Supplementary Figure S3**). On the other hand, the deepening of the fault tip and the development of a wide

FIGURE 15 | Comparison of the ages (vertical bars) and the vertical uplifts (numbers between brackets) for the onshore paleoseismological events (McAuliffe et al., 2015; Rockwell et al., 2016) and offshore deformation uplift events for Ventura-Pitas Point fault (1; profile D01L03 **Figure 9**) and the Ventura Avenue anticline (2; profile D03L03 **Figure 11B**). Horizontal gray bands consider the maximum and minimum ages obtained on the onshore studies for each event, considering that these ages are more reliable than the estimated ages based on the offshore seismic profiles.

southern limb of the Ventura-Avenue anticline (Sorlien and Nicholson, 2015) could distribute the deformation on a wider area, which would also explain the observed decrease in deformation. The CHIRP data reveal that the oldest offshore event shows half of the vertical uplift as the previous two events. Although there are no available age data to constrain the age of the different sedimentary units and the timing of the uplift events, their approximate age can be estimated following the explained approach to calculate the Holocene sedimentation rates and, thus obtain the minimum and maximum age of the different event horizons. The calculated sedimentations rates on profile D01L03 (**Figure 9** and **Supplementary Table S1**) range between 3.3 and 3.9 mm/yr and the age for Event Horizon 1 ranges between 793 and 997 yr ago, Event Horizon 2 between 1969 and 2494 yr ago, and Event Horizon 3 between 3134 and 3888 yr ago (**Figure 15** and **Supplementary Table S2**). Accordingly, event 1 may correlate with the most recent event interpreted by McAuliffe et al. (2015). Events 2 and 3 cannot be directly correlated with any onshore event interpreted in Ventura-Pitas Point fault. Even though, event 3 has an estimated age slightly younger than the onshore event 2, given all the uncertainties related to the estimation of the sedimentation rates and the event horizon ages it could correlate to onshore event 2 (i.e., no compaction considered, constant sedimentation rate or a nominal interval velocity of 1500 m/s TWTT to convert time to depth). Offshore event 2 is not observed onshore at the Ventura-Pitas Point fault site maybe because there is a condensed sedimentary section onshore that failed to record this event.

Rockwell et al. (2016) described four generations of emergent marine terraces between Punta Gorda and Ventura with the

oldest one uplifted a minimum of 38 m in the last 7000 yr. Each of these terraces were interpreted to be associated with a coseismic uplift event on the Ventura-Avenue anticline, and therefore the underlying Ventura-Pitas Point fault (Rockwell et al., 2016). The analysis and dating of the different terraces determined that the two most recent events occurred between 820 and 1060 yr BP, with a preferred age of 955 yr BP, and between 1915 and 2155 yr BP, with a preferred age of 2090 yr BP. The older event produced uplifts between 5 and 10 m, with the earlier event potentially being slightly larger (**Figure 15**). In comparison, the two older events uplifted the terraces 10–12 m and took place between 4215 and 4705 yr BP and between 6600 and 6825 yr BP (**Figure 15**). Evidence for at least three, maybe four, uplift events are observed in the CHIRP profiles across the Ventura-Avenue anticline (**Figure 11**). The uplifts estimated offshore are lower than those reported onshore, similar to the case for the Ventura-Pitas Point fault. The reasons for the decrease uplift may be the same as suggested previously. Nevertheless, the datasets show that the Ventura-Avenue anticline may become less active towards the west where approaching the Red Mountain anticline (**Figure 3**) suggesting that towards the west the system would accommodate more deformation in the nearshore structures. Comparing the relative uplift between events onshore and offshore, we observed that the offshore uplift produced in event 1 (0.4–0.6 m) is slightly lower than in event 2 (0.3–1.1 m) (**Figure 15**). Event 3 shows the least amount of uplift (0.2–0.6 m) of the three events offshore, which is not consistent with the results reported onshore, although it is possible that much of the strain could have been transferred to the Red Mountain and Rincon Creek structures. There are other structures in the area (subtle anticline, offset 1250, in

Figure 11B); however, suggesting that the deformation could be accommodated across a larger area. Although with much uncertainty, a fourth and older event is observed in the CHIRP seismic data (offset 2950, **Figure 11B**) and might correlate with the oldest event identified onshore (Rockwell et al., 2016). If so, although no age data are available for the area, we have estimated the possible minimum and maximum ages for the different event horizons following the same approach employed for the Ventura-Pitas Point fault. On profile D03L03 (**Figure 11B**), the sedimentations rates range between 2.4 and 2.8 mm/yr (**Supplementary Table S1**), lower than in profile D01L03 suggesting that the sedimentation rates are not uniform across all the area. The estimated age for Event Horizon 1 ranges between 1190 and 1483 yr, for Event Horizon 2 between 2064 and 2676 yr, and for Event Horizon 3 between 3587 and 4596 yr (**Figure 15** and **Supplementary Table S3**). The comparison of these ages with the event ages provided for the marine terraces uplift events (Rockwell et al., 2016) shows that the ranges obtained for event horizons 2 and 3 partially overlap with the onshore events 2 and 3 (**Figure 15**). In contrast, Event Horizon 1 cannot be directly correlated with the onshore event 1 since the offshore age is slightly older. Nevertheless, taking into account the uncertainties in the estimation of the sedimentation rates and the horizon event ages, it cannot be ruled out that they correspond to the same event (event 1).

As noted above, the numbers of events interpreted offshore is roughly consistent with the events observed onshore and can be correlated along the same structures. Accordingly, since the onshore events have been interpreted as paleoearthquakes, the deformation uplift events interpreted offshore may also be associated to coseismic deformation and, thus, the event horizons may indicate the time of occurrence of paleoearthquakes. In addition, a general comparison provides a more regional event correlation. The uncertainty in the age of the most recent event, event 1, thus it could correlate with either the Ventura-Pitas Point fault or the Ventura-Avenue anticline (McAuliffe et al., 2015; Rockwell et al., 2016). Although, in the offshore part of the Ventura-Avenue anticline the estimated age is older for this event, it is plausible that it would represent the offshore deformation related to the youngest event. The age ranges estimated for the second event in the offshore Ventura-Pitas Point fault and the Ventura-Avenue anticline overlap quite well (**Figure 15**). This suggests that this event may correlate with the Ventura-Pitas Point fault, although no evidences have been observed in the onshore studies (McAuliffe et al., 2015). According to the obtained age ranges, the third event can be correlated between both deformation zones, onshore and offshore, although the age obtained in the offshore Ventura-Pitas Point fault is slightly younger (**Figure 15**). Despite much uncertainty in the chronology based on sedimentation rates, the three events observed offshore Ventura-Pitas Point fault and Ventura-Avenue anticline appear to correlate roughly with the events documented onshore (McAuliffe et al., 2015; Rockwell et al., 2016). Finally, the possible coincidence in time of the events in both structures may suggest that large earthquakes may rupture both the Ventura-Pitas Point fault and Ventura-Avenue anticline at the same time.

Potential Seismic and Tsunami Hazards

The different fault systems mapped and analyzed in the offshore between Ventura and Santa Barbara show evidence for a similar number of deformation uplift and folding events since the formation of the LGTS: *1*) three events in the Ventura-Pitas Point fault; *2*) three, potentially four, in the Ventura-Avenue anticline; and *3*) four in the Red Mountain anticline, and in the frontal anticline of the Mesa-Rincon Creek fold system and in its back-thrust. In compressional tectonic environments, earthquakes ruptures may not reach the surface when they are nucleating in deeper areas of the seismogenic zone (i.e., blind thrusts). Nevertheless, the deformation associated with blind-thrusting can result in the folding of the shallowest units producing fault-propagation folds and fault-bend folds (Fossen, 2016). The geometrical models of these types of folding show that the size of the areas affected by folding depends on the depth and dip of the fault and the amount of slip. Coseismic folding may result in tilting movements of the ground surface and vertical displacement, of up to several meters for very large earthquakes. This surface deformation may result in the preservation of evidence of the coseismic folding in the geological record as stratigraphic unconformities, difference in thickness along a unit or erosional truncations (McCalpin and Carver, 2009). As previously described, we have identified different angular unconformities, growth strata, reflectors onlaps and different degree of folding associated to the different deformation uplift events. Accordingly, the different interpreted events occurred in the analyzed fault and fold systems may be interpreted as related to coseismic deformation. This is also supported by the good correlation between the events observed onshore and offshore for the Ventura-Pitas Point fault and the Ventura-Avenue anticline. Despite a poor chronostratigraphic framework in the offshore region, the identification of a similar number of uplift events or earthquakes along different fault systems suggests a possible fault interaction and could support two different scenarios: *1*) earthquake triggering, where the occurrence of one event triggers the next rupture close in time; or *2*) a simultaneous rupture of all the faults during larger events. The two scenarios have different implications for the seismic hazard in the area.

In the first scenario, considering that each fault is producing an independent event and their total length represents the maximum surface rupture length, we would expect maximum earthquakes in the range of Mw 6.7–7.0 (Wells and Coppersmith, 1994; Wesnousky, 2008). The occurrence of a rupture on a fault could trigger ruptures on nearby faults due to changes in the Coulomb static stress (Stein et al., 1997; Harris, 2000; Lin and Stein, 2004; Martínez-Díaz et al., 2004; Freed et al., 2007; Heidbach and Ben-Avraham, 2007; Ortuño et al., 2008; Perea, 2009; Brothers et al., 2011; Sahakian et al., 2016; Kariche et al., 2018). This is a plausible hypothesis given the blind thrusts may coalesce into a common master detachment as proposed in this work and in other studies (Hubbard et al., 2014; Levy et al., 2019). Accordingly, a clustering of earthquakes in time would be expected.

The second scenario considers a multifault rupture involving the rupture of all faults during one large event. This scenario

would imply that the slip can jump from one fault to another linking all the faults in the area between Ventura and Point Conception for a total rupture length of approximately 125 km. Such a rupture could produce a maximum earthquake of Mw 7.4–7.9 (Wells and Coppersmith, 1994; Wesnousky, 2008). The 2016 Kaikoura earthquake (Mw 7.8) was a multifault, complex rupture event that involved 21 faults along approximately 180 km of fault length with maximum displacements between 0.7 and 11 m, mainly right-lateral and reverse (Clark et al., 2017; Hamling et al., 2017; Kaiser et al., 2017; Stirling et al., 2017; Litchfield et al., 2018). Rupture process and slip distribution models based on seismic, GPS and InSAR data have shown that to explain this complexity in the rupture it is required to produce slip along a deep detachment, a crustal thrust fault or a subduction interface, where the strike-slip faults may branch out (Cesca et al., 2017; Wang et al., 2018). Considering that the main blind thrusts in the Ventura and Inner Santa Barbara Basins could be branching from a common master detachment (Hubbard et al., 2014; Levy et al., 2019), a large magnitude earthquake involving the rupture along all the different fault systems in the area could be also expected.

The maximum single-event vertical uplift offshore reaches 10–11 m in the frontal blind thrust of the Mesa-Rincon Creek fold system, which is similar to the estimated displacement based on the marine terraces in the Ventura-Avenue anticline by Rockwell et al. (2016). Historical earthquakes with uplifts similar to those observed for the Ventura-Avenue anticline (Rockwell et al., 2016) are associated with large magnitude earthquakes. For example, the 1999 Chi-Chi, Mw 7.6, had 7.5–10 m maximum uplift and ~100 km rupture length (Lin et al., 2001; Rubin et al., 2001) and the 2008 Wenchuan, Mw 7.9, had 10 m uplift and ~250 km rupture length (Parsons et al., 2008; Liu-Zeng et al., 2009). Given the potential of large magnitude earthquakes in this region, the rapid uplift of the seafloor of ~10 m could be tsunamigenic, which could impact the coastal areas between Ventura and Santa Barbara as shown by numerical modelling (Ryan et al., 2015).

CONCLUSIONS

Examination of high-resolution CHIRP profiles in the Offshore Ventura and Inner Santa Barbara basins identified the LGTS and two major Holocene units. Deformation of the LGTS and observed onlapping packages across the active structures provide evidence for three to four Holocene paleoearthquakes. Age estimates for the events based on the depth of the LGTS and the Holocene sediment thickness show rough correlation with the onshore paleoseismological results for the Ventura-Pitas Point fault and the Ventura-Avenue Anticline. The main results of this study are the following:

1. Onshore-offshore correlation of the active structures shows that the Ventura-Pitas Point fault, the Ventura-Avenue anticline, and the Mesa-Rincon Creek fold system extend towards the west offshore. In contrast to previous onshore-offshore correlations, our interpretation suggests that there is

not a direct connection between the onshore Red Mountain fault and the offshore Red Mountain anticline. The Red Mountain anticline is clearly imaged in the seismic data, and its trend changes from E-W to NE-SW where it approaches Rincon Point and aligns with the NE-SW trending Rincon Creek. We propose that a tear-fault or a lateral ramp controls the trend of the creek and structurally separates both structures.

2. The magnitude of Holocene deformation associated with the offshore structures systematically diminishes to the west away from Ventura and Carpinteria. For example, the decrease in observed deformation on one structure (e.g., Ventura-Avenue anticline) correlates with an increase in deformation observed on the adjacent northern structure (e.g., Red Mountain anticline), suggesting an out-of-sequence propagation of the deformation in the thrust system. One potential explanation is that the sea level rise after the LGM has increased the normal stress on the frontal structures in the offshore region, thereby causing the deformation front to step north toward the hinterland.

3. According to the different deformation characteristics observed on the LGTS, we propose that the main thrust faults dip towards the north with decreasing dip at depth. These frontal thrusts could link with a common master detachment at depth. Associated with some of the frontal main thrusts, there are shallow back thrusts that may dip steeper than the main thrusts and towards the south. A common master detachment may explain the migration of the strain to the hinterland structures during the Holocene.

4. Given the similar number of deformation uplift events observed on the Ventura-Pitas Point fault, the Ventura Avenue anticline, the Red Mountain anticline, and the Mesa-Rincon fault system, and interpreted as coseismic deformation, suggests it is possible that the different segments could all rupture in concert with large vertical uplifts per event (up to 10 m). Such an event could produce a large earthquake (>Mw 7.5) with attendant severe ground motion and could be tsunamigenic.

These results provide critical information about the active structures in the offshore areas of the Western Transverse Ranges, their link to the onshore events, and characterize the recency of deformation. Future coring expeditions could improve the chronostragraphic framework in the region and refine the ages of the offshore events. Such studies focused on characterizing the surface deformation in the offshore areas provide important constraints to assess the potential hazards for the region and show the importance of carrying these type of research in other areas.

DATA AVAILABILITY STATEMENT

The original contributions presented in the study are included in the article/**Supplementary Material**, further inquiries can be directed to the corresponding authors.

AUTHOR CONTRIBUTIONS

FUNDING

SUPPLEMENTARY MATERIAL

The Supplementary Material for this article can be found online at: https://www.frontiersin.org/articles/10.3389/feart.2021.655339/full#supplementary-material

REFERENCES

Ammon, C. J., Ji, C., Thio, H.-K., Robinson, D., Ni, S., Hjörleifsdóttir, V., et al. (2005). Rupture Process of the 2004 Sumatra-Andaman Earthquake. *Science.* 308, 1133–1139. doi:10.1126/science.1112260

Armijo, R., Pondard, N., Meyer, B., Uçarkus, G., de Lépinay, B. M., Malavieille, J., et al. (2005). Submarine Fault Scarps in the Sea of Marmara Pull-Apart (North Anatolian Fault): Implications for Seismic Hazard in Istanbul. *Geochemistry, Geophys. Geosystems.* 6. doi:10.1029/2004gc000896

Azor, A., Keller, E. A., and Yeats, R. S. (2002). Geomorphic Indicators of Active Fold Growth: South Mountain-Oak Ridge Anticline, Ventura Basin, Southern California. *Geol. Soc. Am. Bull.* 114, 745–753. doi:10.1130/0016-7606(2002)114<0745:gioafg>2.0.co;2

Barnes, P. M., and Pondard, N. (2010). Derivation of Direct On-Fault Submarine Paleoearthquake Records From High-Resolution Seismic Reflection Profiles: Wairau Fault, New Zealand. *Geochemistry, Geophys. Geosystems.* 11. doi:10.1029/2010gc003254

Barnes, P. M. (2009). Postglacial (After 20 Ka) Dextral Slip Rate of the Offshore Alpine Fault, New Zealand. *Geology.* 37, 3–6. doi:10.1130/G24764A.1

Bilham, R. (2005). A Flying Start, Then a Slow Slip. *Science.* 308, 1126–1127. doi:10.1126/science.1113363

Brothers, D., Kilb, D., Luttrell, K., Driscoll, N., and Kent, G. (2011). Loading of the San Andreas Fault by Flood-Induced Rupture of Faults beneath the Salton Sea. *Nat. Geosci.* 4, 486–492. doi:10.1038/ngeo1184

Brothers, D. S., Driscoll, N. W., Kent, G. M., Harding, a. J., Babcock, J. M., and Baskin, R. L. (2009). Tectonic Evolution of the Salton Sea Inferred From Seismic Reflection Data. *Nat. Geosci.* 2, 581–584. doi:10.1038/ngeo590

Cesca, S., Zhang, Y., Mouslopoulou, V., Wang, R., Saul, J., Savage, M., et al. (2017). Complex Rupture Process of the Mw 7.8, 2016, Kaikoura Earthquake, New Zealand, and its Aftershock Sequence. *Earth Planet. Sci. Lett.* 478, 110–120. doi:10.1016/j.epsl.2017.08.024

Clark, K. J., Nissen, E. K., Howarth, J. D., Hamling, I. J., Mountjoy, J. J., Ries, W. F., et al. (2017). Highly Variable Coastal Deformation in the 2016 MW7.8 Kaikōura Earthquake Reflects Rupture Complexity Along a Transpressional Plate Boundary. *Earth Planet. Sci. Lett.* 474, 334–344. doi:10.1016/j.epsl.2017.06.048

Dahlen, M. Z., Osborne, R. H., and Gorsline, D. S. (1990). Late Quaternary History of the Ventura Mainland Shelf, California. *Mar. Geology.* 94, 317–340. doi:10.1016/0025-3227(90)90062-O

Dibblee, T. W. (1982). "Geology of the Santa Ynez-Topatopa Mountains, Southern California," in *Geology and Mineral Wealth of the California Transverse Ranges.* Editors D. L. Fife and J. H. Minch (Santa Ana, CA: South Coast Geological Society), 41–56. Available at: http://southcoastgeo.org/.

Dolan, J. F., and Rockwell, T. K. (2001). Paleoseismologic Evidence for a Very Large (Mw >7), Post-A.D. 1660 Surface Rupture on the Eastern San Cayetano Fault, Ventura County, California: Was This the Elusive Source of the Damaging 21 December 1812 Earthquake? *Bull. Seismological Soc. America.* 91, 1417–1432. doi:10.1785/0120000602

Donnellan, A., Hager, B. H., and King, R. W. (1993a). Discrepancy Between Geological and Geodetic Deformation Rates in the Ventura Basin. *Nature.* 366, 333–336. doi:10.1038/366333a0

Donnellan, A., Hager, B. H., King, R. W., and Herring, T. A. (1993b). Geodetic Measurement of Deformation in the Ventura Basin Region, Southern California. *J. Geophys. Res.* 98, 21727–21739. doi:10.1029/93JB02766

Escartín, J., Leclerc, F., Olive, J.-A., Mevel, C., Cannat, M., Petersen, S., et al. (2016). First Direct Observation of Coseismic Slip and Seafloor Rupture Along a Submarine Normal Fault and Implications for Fault Slip History. *Earth Planet. Sci. Lett.* 450, 96–107. doi:10.1016/j.epsl.2016.06.024

Fairbanks, R. G. (1989). A 17,000-Year Glacio-Eustatic Sea Level Record: Influence of Glacial Melting Rates on the Younger Dryas Event and Deep-Ocean Circulation. *Nature.* 342, 637–642. doi:10.1038/342637a0

Fischer, P. J. (1976). "Late Neogene-Quaternary Tectonics and Depositional Environments of the Santa Barbara Basin, California," in *The Neogene Symposium.* Editors A. E. Fritsche, H. Ter BestJr, and W. W. Wornardt, 33–52.

Fossen, H. (2016). *Structural Geology.* Cambridge, UK: Cambridge University Press. doi:10.1017/9781107415096

Freed, A. M., Ali, S. T., and Bürgmann, R. (2007). Evolution of Stress in Southern California for the Past 200 Years From Coseismic, Postseismic and Interseismic Stress Changes. *Geophys. J. Int.* 169, 1164–1179. doi:10.1111/j.1365-246X.2007.03391.x

Gràcia, E., Grevemeyer, I., Bartolomé, R., Perea, H., Martínez-Loriente, S., Gómez de la Peña, L., et al. (2019). Earthquake Crisis Unveils the Growth of an Incipient continental Fault System. *Nat. Commun.* 10, 3482. doi:10.1038/s41467-019-11064-5

Grigsby, F. B. (1986). *Quaternary Tectonics of the Rincon and San Miguelito Oil fields Area, Western Ventura Basin, California.* Corvallis, OR: Oregon State University.

Gurrola, L. D., Keller, E. A., Chen, J. H., Owen, L. A., and Spencer, J. Q. (2014). Tectonic Geomorphology of Marine Terraces: Santa Barbara Fold Belt, California. *Geol. Soc. America Bull.* 126, 219–233. doi:10.1130/B30211.1

Hager, B. H., Lyzenga, G. a., Donnellan, A., and Dong, D. (1999). Reconciling Rapid Strain Accumulation With Deep Seismogenic Fault Planes in the Ventura Basin, California. *J. Geophys. Res.* 104, 25207–25219. doi:10.1029/1999JB900184

Hamling, I. J., Hreinsdóttir, S., Clark, K., Elliott, J., Liang, C., Fielding, E., et al. (2017). Complex Multifault Rupture During the 2016Mw7.8 Kaikōura Earthquake, New Zealand. *Science.* 356, eaam7194. doi:10.1126/science.aam7194

Harris, R. A. (2000). Earthquake Stress Triggers, Stress Shadows, and Seismic Hazard. *Curr. Sci.* 79, 1215–1225. doi:10.1016/S0074-6142(03)80187-0

Heidbach, O., and Ben-Avraham, Z. (2007). Stress Evolution and Seismic Hazard of the Dead Sea Fault System. *Earth Planet. Sci. Lett.* 257, 299–312. doi:10.1016/j.epsl.2007.02.042

Hoyt, D. (1976). *Geology and Recent Sediment Distribution from Santa Barbara to Rincon Point, California.* Master's thesis. San Diego, CA: San Diego State University.

Hubbard, J., Shaw, J. H., Dolan, J., Pratt, T. L., McAuliffe, L., and Rockwell, T. K. (2014). Structure and Seismic Hazard of the Ventura Avenue Anticline and Ventura Fault, California: Prospect for Large, Multisegment Ruptures in the Western Transverse Ranges. *Bull. Seismological Soc. America.* 104, 1070–1087. doi:10.1785/0120130125

Huftile, G. J., and Yeats, R. S. (1995). Convergence Rates Across a Displacement Transfer Zone in the Western Transverse Ranges, Ventura basin, California. *J. Geophys. Res.* 100, 2043–2067. doi:10.1029/94JB02473

Hughes, A., Rood, D. H., Whittaker, A. C., Bell, R. E., Rockwell, T. K., Levy, Y., et al. (2018). Geomorphic Evidence for the Geometry and Slip Rate of a Young, Low-Angle Thrust Fault: Implications for hazard Assessment and Fault Interaction in Complex Tectonic Environments. *Earth Planet. Sci. Lett.* 504, 198–210. doi:10.1016/j.epsl.2018.10.003

Hutton, K., Woessner, J., and Hauksson, E. (2010). Earthquake Monitoring in Southern California for Seventy-Seven Years (1932-2008). *Bull. Seismological Soc. America.* 100, 423–446. doi:10.1785/0120090130

Hutton, L. K., Jones, L. M., Hauksson, E., and Given, D. D. (1991). "Seismotectonics of Southern California," in *Neotectonics of North America.* Editors D. B. Slemmons, E. R. Engdahl, M. D. Zoback, and D. D. Blackwell (Boulder, CO: Geological Society of America), 133–152. doi:10.1130/DNAG-CSMS-NEO.133

Ide, S., Baltay, A., and Beroza, G. C. (2011). Shallow Dynamic Overshoot and Energetic Deep Rupture in the 2011 Mw 9.0 Tohoku-Oki Earthquake. *Science.* 332, 1426–1429. doi:10.1126/science.1207020

Jackson, P. A. (1981). *Structural Evolution of the Carpinteria Basin, Western Transverse Ranges, California.* Master's thesis. Corvallis, OR: Oregon State University.

Jackson, P. A., and Yeats, R. S. (1982). Structural Evolution of the Carpinteria Basin, Western Transverse Ranges, California. *Am. Assoc. Pet. Geol. Bull.* 66, 805–829. doi:10.1306/03b5a33b-16d1-11d7-8645000102c1865d

Jennings, C. W., and Bryant, W. A. (2010). *Fault Activity Map of California - Data Map No. 6 (Map Scale 1:750,000).* Sacramento, CA: California Department of Conservation. Available at: https://maps.conservation.ca.gov/cgs/fam/

Johnson, S. Y., Cochrane, G. R., Golden, N. E., Dartnell, P., Hartwell, S. R., Cochran, S. A., et al. (2017a). The California Seafloor and Coastal Mapping Program - Providing Science and Geospatial Data for California's State Waters. *Ocean Coastal Management.* 140, 88–104. doi:10.1016/j.ocecoaman.2017.02.004

Johnson, S. Y., Hartwell, S. R., Sorlien, C. C., Dartnell, P., and Ritchie, A. C. (2017b). Shelf Evolution Along a Transpressive Transform Margin, Santa Barbara Channel, California. *Geosphere.* 13, 2041–2077. doi:10.1130/GES01387.1

Kaiser, A., Balfour, N., Fry, B., Holden, C., Litchfield, N., Gerstenberger, M., et al. (2017). The 2016 Kaikōura, New Zealand, Earthquake: Preliminary Seismological Report. *Seismological Res. Lett.* 88, 727–739. doi:10.1785/0220170018

Kariche, J., Meghraoui, M., Timoulali, Y., Cetin, E., and Toussaint, R. (2018). The Al Hoceima Earthquake Sequence of 1994, 2004 and 2016: Stress Transfer and Poroelasticity in the Rif and Alboran Sea Region. *Geophys. J. Int.* 212, 42–53. doi:10.1093/gji/ggx385

Lay, T., Kanamori, H., Ammon, C. J., Nettles, M., Ward, S. N., Aster, R. C., et al. (2005). The Great Sumatra-Andaman Earthquake of 26 December 2004. *Science.* 308, 1127–1133. doi:10.1126/science.1112250

Levy, Y., Rockwell, T. K., Shaw, J. H., Plesch, A., Driscoll, N. W., and Perea, H. (2019). Structural Modeling of the Western Transverse Ranges: An Imbricated Thrust Ramp Architecture. *Lithosphere.* 11, 868–883. doi:10.1130/L1124.1

Lin, A., Ouchi, T., Chen, A., and Maruyama, T. (2001). Co-seismic Displacements, Folding and Shortening Structures Along the Chelungpu Surface Rupture Zone Occurred During the 1999 Chi-Chi (Taiwan) Earthquake. *Tectonophysics.* 330, 225–244. doi:10.1016/S0040-1951(00)00230-4

Lin, J., and Stein, R. S. (2004). Stress Triggering in Thrust and Subduction Earthquakes and Stress Interaction Between the Southern San Andreas and Nearby Thrust and Strike-Slip Faults. *J. Geophys. Res.* 109, B02303. doi:10.1029/2003JB002607

Lindvall, S., Huftile, G. J., Gurrola, L. D., Anderson, L., and Bell, M. A. (2002). *Paleoseismic Investigation of the Red Mountain Fault: Analysis of the Displaced Punta Gorda Marine Terrace.* Santa Ana, CA: South Coast Geological Society, Filed Trip Guidebook. Available at: http://southcoastgeo.org/

Litchfield, N. J., Villamor, P., Dissen, R. J. V., Nicol, A., Barnes, P. M., and Barrell, D. J. A. (2018). Surface Rupture of Multiple Crustal Faults in the 2016 Mw 7.8 Kaikōura, New Zealand, Earthquake. *Bull. Seismol. Soc. Am.* 108, 1496–1520. doi:10.1785/0120170300

Liu-Zeng, J., Zhang, Z., Wen, L., Tapponnier, P., Sun, J., Xing, X., et al. (2009). Co-Seismic Ruptures of the 12 May 2008, Ms 8.0 Wenchuan Earthquake, Sichuan: East–West Crustal Shortening on Oblique, Parallel Thrusts Along the Eastern Edge of Tibet. *Earth Planet. Sci. Lett.* 286, 355–370. doi:10.1016/j.epsl.2009.07.017

Luttrell, K., and Sandwell, D. (2010). Ocean Loading Effects on Stress at Near Shore Plate Boundary Fault Systems. *J. Geophys. Res.* 115, B08411. doi:10.1029/2009JB006541

Marshall, S. T., Funning, G. J., and Owen, S. E. (2013). Fault Slip Rates and Interseismic Deformation in the Western Transverse Ranges, California. *J. Geophys. Res. Solid Earth.* 118, 4511–4534. doi:10.1002/jgrb.50312

Martínez-Díaz, J. J., Álvarez-Gómez, J. A., Benito, B., and Hernández, D. (2004). Triggering of Destructive Earthquakes in El Salvador. *Geology.* 32, 65. doi:10.1130/g20089.1

McAuliffe, L. J., Dolan, J. F., Rhodes, E. J., Hubbard, J., Shaw, J. H., and Pratt, T. L. (2015). Paleoseismologic Evidence for Large-Magnitude (M W 7.5–8.0) Earthquakes on the Ventura Blind Thrust Fault: Implications for Multifault Ruptures in the Transverse Ranges of Southern California. *Geosphere.* 11, 1629–1650. doi:10.1130/GES01123.1

McCalpin, J. P., and Carver, G. A. (2009). "Paleoseismology of Compressional Tectonic Environments," in *Paleoseismology.* Editor J. P. McCalpin (Burlington, ON: Academic Press), 315–419. doi:10.1016/s0074-6142(09)95005-7

McNeill, L. C., Cotterill, C. J., Bull, J. M., Henstock, T. J., Bell, R., and Stefatos, A. (2007). Geometry and Slip Rate of the Aigion Fault, A Young Normal Fault System in the Western Gulf of Corinth. *Geology.* 35, 355. doi:10.1130/g23281a.1

McNeill, L. C., and Henstock, T. J. (2014). Forearc Structure and Morphology Along the Sumatra-Andaman Subduction Zone. *Tectonics.* 33, 112–134. doi:10.1002/2012TC003264

Muhs, D. R., Simmons, K. R., Schumann, R. R., Groves, L. T., DeVogel, S. B., Minor, S. A., et al. (2014). Coastal Tectonics on the Eastern Margin of the Pacific Rim: Late Quaternary Sea-Level History and Uplift Rates, Channel Islands National Park, California, USA. *Quat. Sci. Rev.* 105, 209–238. doi:10.1016/j.quascirev.2014.09.017

Namson, J., and Davis, T. (1988). Structural Transect of the Western Transverse Ranges, California: Implications for Lithospheric Kinematics and Seismic Risk Evaluation. *Geology.* 16, 675. doi:10.1130/0091-7613(1988)016<0675:stotwt>2.3.co;2

National Geophysical Data Center (2012). U.S. Coastal Relief Model - Southern California Version 2. National Geophysical Data Center, NOAA. doi:10.7289/V5V985ZM

Neves, M. C., Cabral, J., Luttrell, K., Figueiredo, P., Rockwell, T., and Sandwell, D. (2015). The Effect of Sea Level Changes on Fault Reactivation Potential in Portugal. *Tectonophysics.* 658, 206–220. doi:10.1016/j.tecto.2015.07.023

Nicholson, C., Sorlien, C. C., Atwater, T., Crowell, J. C., and Luyendyk, B. P. (1994). Microplate Capture, Rotation of the Western Transverse Ranges, and Initiation of the San Andreas Transform as a Low-Angle Fault System. *Geology.* 22, 491. doi:10.1130/0091-7613(1994)022<0491:mcrotw>2.3.co;2

Nicholson, C., Sorlien, C. C., Hopps, T. E., and Kamerling, M. J. (2016). *Anomalous Uplift at Pitas Point: Localized Phenomena or Indicator of Tsunamigenic M8 Earthquakes along Coastal California.* San Francisco, CA: AGU Fall Meeting, 15–19.

Olson, D. J. (1983). *Surface and Subsurface Geology of the Santa Barbara–Goleta Metropolitan Area.* Master's Thesis; Santa Barbara County, CA: Oregon State University.

Ortuño, M., Queralt, P., Martí, A., Ledo, J., Masana, E., Perea, H., et al. (2008). The North Maladeta Fault (Spanish Central Pyrenees) as the Vielha 1923 Earthquake Seismic Source: Recent Activity Revealed by Geomorphological and Geophysical Research. *Tectonophysics.* 453, 246–262. doi:10.1016/j.tecto.2007.06.016

Ozawa, S., Nishimura, T., Suito, H., Kobayashi, T., Tobita, M., and Imakiire, T. (2011). Coseismic and Postseismic Slip of the 2011 Magnitude-9 Tohoku-Oki Earthquake. *Nature.* 475, 373–376. doi:10.1038/nature10227

Parsons, T., Ji, C., and Kirby, E. (2008). Stress Changes From the 2008 Wenchuan Earthquake and Increased Hazard in the Sichuan Basin. *Nature.* 454, 509–510. doi:10.1038/nature07177

Perea, H. (2009). The Catalan Seismic Crisis (1427 and 1428; NE Iberian Peninsula): Geological Sources and Earthquake Triggering. *J. Geodyn.* 47, 259–270. doi:10.1016/j.jog.2009.01.002

Perea, H., Gràcia, E., Alfaro, P., Bartolomé, R., Lo Iacono, C., Moreno, X., et al. (2012). Quaternary Active Tectonic Structures in the Offshore Bajo Segura

basin (SE Iberian Peninsula – Mediterranean Sea). *Nat. Hazards Earth Syst. Sci.* 12, 3151–3168. doi:10.5194/nhess-12-3151-2012

Perea, H., Gràcia, E., Martínez-Loriente, S., Bartolome, R., de la Peña, L. G., de Mol, B., et al. (2018). Kinematic Analysis of Secondary Faults Within a Distributed Shear-Zone Reveals Fault Linkage and Increased Seismic Hazard. *Mar. Geol.* 399, 23–33. doi:10.1016/j.margeo.2018.02.002

Plesch, A., Shaw, J. H., Benson, C., Bryant, W. A., Carena, S., Cooke, M., et al. (2007). Community Fault Model (CFM) for Southern California. *Bull. Seismol. Soc. Am.* 97, 1793–1802. doi:10.1785/0120050211

Polonia, A., Torelli, L., Gasperini, L., and Mussoni, P. (2012). Active Faults and Historical Earthquakes in the Messina Straits Area (Ionian Sea). *Nat. Hazards Earth Syst. Sci.* 12, 2311–2328. doi:10.5194/nhess-12-2311-2012

Reeder-Myers, L., Erlandson, J. M., Muhs, D. R., and Rick, T. C. (2015). Sea Level, Paleogeography, and Archeology on California ' S Northern Channel Islands. *Quat. Res.* 83, 263–272. doi:10.1016/j.yqres.2015.01.002

Reynolds, L. C., and Simms, A. R. (2015). Late Quaternary Relative Sea Level in Southern California and Monterey Bay. *Quat. Sci. Rev.* 126, 57–66. doi:10.1016/j.quascirev.2015.08.003

Rockwell, T. K., Clark, K., Gamble, L., Oskin, M. E., Haaker, E. C., and Kennedy, G. L. (2016). Large Transverse Range Earthquakes Cause Coastal Upheaval Near Ventura, Southern California. *Bull. Seismol. Soc. Am.* 106, 2706–2720. doi:10.1785/0120150378

Rockwell, T. K., Keller, E. A., and Dembroff, G. R. (1988). Quaternary Rate of Folding of the Ventura Avenue Anticline, Western Transverse Ranges, Southern California. *Bull. Geol. Soc. Am.* 100, 850–858. doi:10.1130/0016-7606(1988)100<0850:qrofot>2.3.co;2

Rockwell, T. K. (1988). Neotectonics of the San Cayetano Fault, Transverse Ranges, California. *Geol. Soc. Am. Bull.* 100, 500–513. doi:10.1130/0016-7606(1988)100<0500:NOTSCF>2.310.1130/0016-7606(1988)100<0500:notscf>2.3.co;2

Rubin, C. M., Sieh, K., Chen, Y. G., Lee, J. C., Chu, H. T., Yeats, R., et al. (2001). Surface Rupture and Behavior of Thrust Faults Probed in Taiwan. *Eos (Washington. DC).* 82, 565–569. doi:10.1029/01EO00331

Ryan, K. J., Geist, E. L., Barall, M., and Oglesby, D. D. (2015). Dynamic Models of an Earthquake and Tsunami Offshore Ventura, California. *Geophys. Res. Lett.* 42, 6599–6606. doi:10.1002/2015GL064507

Sahakian, V., Bormann, J., Driscoll, N., Harding, A., Kent, G., and Wesnousky, S. (2017). Seismic Constraints on the Architecture of the Newport-Inglewood/Rose Canyon Fault: Implications for the Length and Magnitude of Future Earthquake Ruptures. *J. Geophys. Res. Solid Earth* 122, 2085–2105. doi:10.1002/2016JB013467

Sahakian, V., Kell, A., Harding, A., Driscoll, N., and Kent, G. (2016). Geophysical Evidence for a San Andreas Subparallel Transtensional Fault Along the Northeastern Shore of the Salton Sea. *Bull. Seismol. Soc. Am.* 106, 1963–1978. doi:10.1785/0120150350

Sato, M., Ishikawa, T., Ujihara, N., Yoshida, S., Fujita, M., Mochizuki, M., et al. (2011). Displacement Above the Hypocenter of the 2011 Tohoku-Oki Earthquake. *Science.* 332, 1395. doi:10.1126/science.1207401

Sedlock, R. L., and Hamilton, D. H. (1991). Late Cenozoic Tectonic Evolution of Southwestern California. *J. Geophys. Res.* 96, 2325. doi:10.1029/90JB02018

Shaw, J. H., and Suppe, J. (1994). Active Faulting and Growth Folding in the Eastern Santa Barbara Channel, California. *Geol. Soc. Am. Bull.* 106, 607. doi:10.1130/0016-7606(1994)106<0607:afagfi>2.3.co;2

Simons, M., Minson, S. E., Sladen, A., Ortega, F., Jiang, J., Owen, S. E., et al. (2011). The 2011 Magnitude 9.0 Tohoku-Oki Earthquake: Mosaicking the Megathrust from Seconds to Centuries. *Science.* 332, 1421–1425. doi:10.1126/science.1206731

Sliter, R. W., Triezenberg, P. J., Hart, P. E., Draut, A. E., Normark, W. R., and Conrad, J. E. (2008). *High-Resolution Chirp and Mini-Sparker Seismic-Reflection Data from the Southern California Continental Shelf - Gaviota to Mugu Canyon.* Menlo Park, CA: USGS. Available at: https://pubs.usgs.gov/of/2008/1246/index.html.

Sorlien, C. C., Gratier, J.-P., Luyendyk, B. P., Hornafius, J. S., and Hopps, T. E. (2000). Map Restoration of Folded and Faulted Late Cenozoic Strata across the Oak Ridge Fault, Onshore and Offshore Ventura basin, California. *Geol. Soc. Am. Bull.* 112, 1080–1090. doi:10.1130/0016-7606(2000)112<1080:mrofaf>2.0.co;2

Sorlien, C. C., Nicholson, C., Behl, R. J., Marshall, C. J., and Kennett, J. P. (2014). *The Quaternary North Channel-Pitas Point Fault System in Northwest Santa Barbara Channel, California.* San Francisco, CA: AGU Fall Meeting, 15–19.

Sorlien, C. C., and Nicholson, C. (2015). Post-1 Ma Deformation History of the Pitas Point-North Channel-Red Mountain Fault System and Associated Folds

in Santa Barbara Channel, California. Available at: https://earthquake.usgs.gov/cfusion/external_grants/reports/G14AP00012.pdf.

Stanford, J. D., Hemingway, R., Rohling, E. J., Challenor, P. G., Medina-Elizalde, M., and Lester, A. J. (2011). Sea-level Probability for the Last Deglaciation: A Statistical Analysis of Far-Field Records. *Glob. Planet. Change.* 79, 193–203. doi:10.1016/j.gloplacha.2010.11.002

Stein, R. S., Barka, A. A., and Dieterich, J. H. (1997). Progressive Failure on the North Anatolian Fault Since 1939 by Earthquake Stress Triggering. *Geophys. J. Int.* 128, 594–604. doi:10.1111/j.1365-246X.1997.tb05321.x

Stirling, M. W., Litchfield, N. J., Villamor, P., Dissen, R. J. Van, Nicol, A., Pettinga, J., et al. (2017). The Mw7.8 2016 Kaikōura Earthquake: Surface Fault Rupture and Seismic Hazard Context. *Bull. New Zeal. Soc. Earthq. Eng.* 50, 73–84. doi:10.5459/bnzsee.50.2.73-84

Subarya, C., Chlieh, M., Prawirodirdjo, L., Avouac, J.-P., Bock, Y., Sieh, K., et al. (2006). Plate-Boundary Deformation Associated with the Great Sumatra–Andaman Earthquake. *Nature.* 440, 46–51. doi:10.1038/nature04522

Toppozada, T., and Branum, D. (2004). California Earthquake History. *Ann. Geophys.* 47, 509–522. doi:10.4401/ag-3317

Toppozada, T. R., Branum, D. M., Reichle, M. S., and Hallstrom, C. L. (2002). San Andreas Fault Zone, California: M >=5.5 Earthquake History. *Bull. Seismol. Soc. Am.* 92, 2555–2601. doi:10.1785/0120000614

Wang, T., Wei, S., Shi, X., Qiu, Q., Li, L., Peng, D., et al. (2018). The 2016 Kaikōura Earthquake: Simultaneous Rupture of the Subduction Interface and Overlying Faults. *Earth Planet. Sci. Lett.* 482, 44–51. doi:10.1016/j.epsl.2017.10.056

Wells, D. L., and Coppersmith, K. J. (1994). New Empirical Relationships Among Magnitude, Rupture Length, Rupture Area and Surface Displacement. *Bull. Seismol. Soc. Am.* 84, 974–1002.

Wesnousky, S. G. (2008). Displacement and Geometrical Characteristics of Earthquake Surface Ruptures: Issues and Implications for Seismic-Hazard Analysis and the Process of Earthquake Rupture. *Bull. Seismol. Soc. Am.* 98, 1609–1632. doi:10.1785/0120070111

Yeats, R. S., Huftile, G. J., and Grigsby, F. B. (1988). Oak Ridge Fault, Ventura Fold Belt, and the Sisar Decollement, Ventura Basin, California. *Geology.* 16, 1112. doi:10.1130/0091-7613(1988)016<1112:orfvfb>2.3.co;2

Yeats, R. S., Huftile, G. J., and Stitt, L. T. (1994). Late Cenozoic Tectonics of the East Ventura Basin, Transverse Ranges, California. *Am. Assoc. Pet. Geol. Bull.* 78, 1040–1074. doi:10.1306/A25FE42D-171B-11D7-8645000102C1865D

Yeats, R. S. (1983). Large-scale Quaternary Detachments in Ventura Basin, Southern California. *J. Geophys. Res.* 88, 569. doi:10.1029/JB088iB01p00569

Yeats, R. S., Lee, W. H. K., and Yerkes, R. F. (1987). "Geology and Seismicity of the Eastern Red Mountain Fault, Ventura County," in *Recent Reverse Faulting in the Transverse Ranges.* California: USGS Professional Paper, 1339, 161–168.

Yeats, R. S., and Olson, D. J. (1984). Alternate Fault Model for the Santa Barbara, California, Earthquake of 13 August 1978. *Bull. Seismol. Soc. Am.* 74, 1545–1553. doi:10.1785/BSSA0740051545

Yerkes, R. F., and Lee, W. H. K. (1987). "Late Quaternary Deformation in the Western Transverse Ranges," in *Recent Reverse Faulting in the Transverse Ranges.* California: USGS Professional Paper, 1339, 71–82.

Yerkes, R. F., Sarna-Wojcicki, A. M., and Lajoie, K. R. (1987). "Geology and Quaternary Deformation of the Ventura Area," in *Recent Reverse Faulting in the Transverse Ranges.* California: USGS Professional Paper, 1339, 169–178.